






## Thermal and magnetic properties and optical spectroscopy of $\text{SmCr}_3(\text{BO}_3)_4$

K. N. Boldyrev <sup>1,\*</sup>, N. N. Kuz'min,<sup>1,2,3</sup> A. A. Mukhin,<sup>4</sup> V. Yu. Ivanov,<sup>4</sup> E. A. Dobretsova <sup>4</sup>, E. A. Popova <sup>5</sup>,  
S. Yu. Gavrilkin,<sup>6</sup> N. I. Leonyuk,<sup>2,†</sup> V. V. Maltsev,<sup>2</sup> B. Z. Malkin <sup>7</sup> and M. N. Popova <sup>1</sup>

<sup>1</sup>*Institute of Spectroscopy, Russian Academy of Sciences, Troitsk, Moscow 108840, Russia*

<sup>2</sup>*Moscow State University, Moscow 119991, Russia*

<sup>3</sup>*Moscow Institute of Physics and Technology (National Research University), Dolgoprudnyi 141700, Russia*

<sup>4</sup>*Prokhorov General Physics Institute, Russian Academy of Sciences, Moscow 119991, Russia*

<sup>5</sup>*National Research University Higher School of Economics, Moscow 101000, Russia*

<sup>6</sup>*Lebedev Physical Institute, Russian Academy of Sciences, Moscow 119991, Russia*

<sup>7</sup>*Kazan Federal University, Kazan 420008, Russia*



(Received 22 June 2021; revised 23 September 2021; accepted 6 October 2021; published 29 October 2021)

We measured the heat capacity, magnetic susceptibility, magnetization, magnetoelectric effect, and optical spectra of samarium chromium borate crystals. It was found that, in  $\text{SmCr}_3(\text{BO}_3)_4$  single crystals, structures with the space groups  $R32$  and  $C2/c$  may coexist. Magnetic phase transitions were discovered at temperatures  $T_{N1} = 7.8 \pm 0.5$  K,  $T_{N2} = 6.7 \pm 0.5$  K, and  $T_3 = 4.3 \pm 0.2$  K, and assumptions about their nature were made. Based on the high-resolution optical spectra and magnetometry data, the crystal-field parameters in the  $\text{Sm}^{3+}$  and  $\text{Cr}^{3+}$  positions and the parameters of  $\text{Cr}^{3+}$ - $\text{Cr}^{3+}$  and  $\text{Cr}^{3+}$ - $\text{Sm}^{3+}$  exchange interactions were determined. The magnetic properties of the quasi-one-dimensional chromium subsystem were analyzed in the frame of the previously developed self-consistent four-particle cluster model. Despite a strong suppression of  $\text{Cr}^{3+}$  magnetic moments by the interchain antiferromagnetic exchange interactions, the contributions of the chromium subsystem to the bulk magnetization are dominant.

DOI: [10.1103/PhysRevMaterials.5.104413](https://doi.org/10.1103/PhysRevMaterials.5.104413)

### I. INTRODUCTION

Huntite-family rare earth (RE) borates with the general formula  $RM_3(\text{BO}_3)_4$  ( $R = \text{Y, La-Lu}$ ;  $M = \text{Al, Ga, Fe, Cr, Sc}$ ) crystallize mainly in the trigonal (the structure of the huntite mineral with the space group  $R32$ ) or monoclinic (space groups  $C2/c$  and  $C2$ ) modifications [1–3]. The most famous of them are RE aluminum borates ( $M = \text{Al}$ ). They are characterized by low concentration quenching of luminescence, chemical resistance, and mechanical strength, as well as pronounced nonlinear optical properties and belong to the materials of a new generation for lasers with self-frequency doubling and self-frequency mixing [4,5], mini-lasers [6], high-brightness phosphors [7–9], and visual information systems [10]. Recently, high optical nonlinearity was also found in RE gallium borates [11]. In RE aluminum [12,13], gallium [14], and iron [15–17] borates, a magnetoelectric effect was found, and these compounds can be assigned to a new class of magnetoelectrics; some of them possessing spontaneous electric polarization are multiferroics. The study of multiferroics has attracted an increased interest due to the possibility of controlling the magnetic (electrical) properties using an electric (magnetic) field, which is very valuable for applications, for example, in spintronic devices. Additionally, RE iron borates  $R\text{Fe}_3(\text{BO}_3)_4$  have interesting magnetic properties

due to the presence of two interacting magnetic subsystems (RE and iron). These compounds order antiferromagnetically at temperatures of 20–40 K [18,19], and a wide variety of magnetic structures is observed, depending on the RE ion  $R^{3+}$  and temperature [20].

In connection with the above, it is of interest to study borates with another magnetic ion, chromium. At present, not much is known about the magnetic and other properties of RE chromium borates. X-ray diffraction data and studies of vibrational infrared (IR) spectra have shown that they crystallize in both trigonal  $R32$  and monoclinic  $C2/c$  space groups [21,22]. Earlier, the comprehensive studies of  $\text{NdCr}_3(\text{BO}_3)_4$  crystals were carried out, which showed that the magnetic subsystems of  $\text{Cr}^{3+}$  and  $\text{Nd}^{3+}$  ions antiferromagnetically ordered into an easy-plane magnetic structure at a temperature of  $\sim 8.0$  K [23,24]. In Ref. [24], spectroscopic data were also presented on  $\text{SmCr}_3(\text{BO}_3)_4$ ; they indicated a phase transition at a temperature of  $\sim 5$  K. An antiferromagnetic phase transition at a temperature of  $\sim 9.5$  K was reported for the  $\text{EuCr}_3(\text{BO}_3)_4$  crystal [25]. Recent studies of the magnetic properties of  $\text{GdCr}_3(\text{BO}_3)_4$  [26] and  $\text{TbCr}_3(\text{BO}_3)_4$  [27] crystals revealed antiferromagnetic ordering into an easy-plane structure at temperatures  $T_N = 7.15$  and 8.8 K, respectively. In  $\text{TbCr}_3(\text{BO}_3)_4$ , an additional spin-reorientation transition into the easy-axis phase was observed at a temperature of  $\sim 5$  K [27]. In Ref. [28], based on the analysis of the measured temperature dependence of the magnetic susceptibility of the  $\text{LaCr}_3(\text{BO}_3)_4$  crystal containing coexisting polytypes of trigonal ( $R32$ ) and monoclinic ( $C2/c$ ) structures in a ratio

\*kn.boldyrev@gmail.com

†Deceased.

2:3, it was concluded that the observed two phase transitions at temperatures  $T_N = 8.5$  and  $6.5$  K correspond to magnetic ordering in the two structural modifications. Two magnetic phase transitions at temperatures  $T_N = 9.1$  and  $7.5$  K and a sequence of four spin-reorientation transitions at temperatures  $T_{SR} = 5.7, 5.5, 4.6,$  and  $3.6$  K, associated with changes in the orientation of spontaneous magnetic moments, were observed in a structurally two-phase crystal  $\text{DyCr}_3(\text{BO}_3)_4$  [29].

This paper is devoted to the experimental study of the heat capacity, spectral, magnetic, and magnetoelectric characteristics of  $\text{SmCr}_3(\text{BO}_3)_4$  crystals, as well as theoretical modeling of their optical spectra and magnetic properties. Some preliminary results were presented in Ref. [30]. This paper is organized as follows. In Sec. II, we describe the samples used and the details of calorimetric, magnetic, magnetoelectric, and optical measurements. The structural information is given in Sec. III. Section IV presents the temperature dependences of heat capacity and magnetic susceptibility, field dependences of magnetization, results of the magnetoelectric measurements, and temperature-dependent polarized spectra of  $\text{SmCr}_3(\text{BO}_3)_4$  in the regions of  $f$ - $f$  optical transitions in the  $\text{Sm}^{3+}$  ions and  $d$ - $d$  transitions in the  $\text{Cr}^{3+}$  ions. Section V is devoted to the theoretical consideration of the crystal-field (CF) excitations of the samarium and chromium ions and the magnetic properties of  $\text{SmCr}_3(\text{BO}_3)_4$ . The paper ends with Conclusions.

## II. EXPERIMENT

Crystals of samarium chromium borate of nominal composition and doped with 1% erbium or neodymium introduced as a spectroscopic probe were obtained as a result of spontaneous crystallization from a solution melt based on potassium trimolybdate  $\text{K}_2\text{Mo}_3\text{O}_{10}$  used as a solvent. The mass ratio of borate:solvent in the charge was 1:1. Crystallization of  $\text{SmCr}_3(\text{BO}_3)_4$  took place in the temperature range  $900$ – $950$  °C. These conditions ensured the crystallization mainly of the  $R32$  phase (lattice parameters  $a = 0.949$  nm,  $c = 0.749$  nm) [21,22,31]. Crystals were dark green in color, had a volume of up to  $1$  mm<sup>3</sup> and a clear faceting. The samples were oriented using the crystal morphology and optical polarization methods.

Temperature dependences of heat capacity and magnetic susceptibility and field dependences of magnetization were measured on PPMS-9 and MPMS-5 setups manufactured by Quantum Design (USA). Magnetic measurements were carried out both on a “mosaic” composed of several separate crystals oriented in the same way and on single crystals with masses from  $0.40$  to  $1.73$  mg. The temperature and field dependences of magnetization for both types of samples were qualitatively similar, although there were some quantitative differences due to errors in determining the mass of crystals and an inevitable misorientation of crystals in the mosaic as well as different ratios of the trigonal  $R32$  and monoclinic  $C2/c$  phases in different crystals. The data presented in Sec. IV C refer mainly to one crystal with a mass of  $0.56$  mg.

Electric polarization was studied along the crystallographic  $a$  axis by pyroelectric measurements in the magnetic field using a Keithley 6517A electrometer. Electrical contacts were

attached by Ag paint on the two parallel surfaces. First, we tried to detect any signs of a change in the electric charge with a change in temperature or magnetic field on one single crystal in the  $P_a(B_b)$  geometry. However, due to a very small surface area of the crystal, we failed to clearly distinguish the signal associated with the magnetoelectric interaction against the background of time drift and random charge fluctuations. Therefore, a mosaic was then made up of a sufficiently large number of small crystals glued to the substrate with faces perpendicular to the  $a$  axis and codirectional  $c$  axes. The mosaic was covered with epoxy resin, and after the resin hardened, it was ground on both sides to the crystal edges, after which contacts were applied using a silver paste. Measurements were carried out in the  $P_a(\mathbf{B}\perp c)$  geometry. A poling field was not applied because, by analogy with iron borates, the magnetoelectric effect (both spontaneous and induced by a magnetic field) is determined by internal fields in the non-centrosymmetric crystal and practically does not depend on the external electric fields. The temperature dependence of polarization upon heating or cooling was measured in swiping temperature mode with a rate of about  $1$  K/min, resulting in a small hysteresis of  $<0.1$  K.

Optical transmission spectra were recorded in a wide temperature range ( $3.5$ – $300$  K) on both powdered and oriented single-crystal samples using a Fourier spectrometer Bruker IFS 125 HR. Powdered samples were mixed with polyethylene, pressed into tablets, and placed into a liquid-helium cryostat with mylar windows of the Novosibirsk Design Bureau, to measure vibrational spectra in the far-IR (FIR) spectral region. Single crystals, the plane of which contained the  $c$  axis, were used to measure polarized spectra in the near- and mid-IR regions ( $3000$ – $12\,000$  cm<sup>-1</sup>) in two possible configurations:  $\mathbf{k}\perp c$ ,  $\mathbf{E}\parallel c$  ( $\pi$  polarization), and  $\mathbf{k}\perp c$ ,  $\mathbf{E}\perp c$  ( $\sigma$  polarization). A Cryomech ST403 closed-cycle helium cryostat with the temperature stabilization  $\pm 0.05$  K was used for these measurements.

## III. STRUCTURAL INFORMATION

In Refs. [21,22,31], a thorough study of the formation of trigonal (the  $R32$  space group) and monoclinic (the  $C2/c$  space group) phases during the crystallization of RE chromium borates was performed. It was found that  $\text{SmCr}_3(\text{BO}_3)_4$  can crystallize in both phases, depending on the crystallization conditions. At the mass ratio of borate : solvent 1:1 and crystallization temperature in the range  $900$ – $950$  °C (as in this paper), the  $R32$  phase is formed mainly. However, layers of the  $C2/c$  phase may be present, which is typical for polytypes [22].

The matter is that the two structures are similar (see Fig. 1). Both have similar coordination polyhedra, namely, distorted prisms  $\text{SmO}_6$ , octahedra  $\text{CrO}_6$ , and  $\text{BO}_3$  triangles, arranged into two kinds of layers. In a trigonal  $R32$  structure, identical layers are translated into each other by twofold axes; in a monoclinic  $C2/c$  structure, they are reflected in the center of inversion [21,22]. However, during the crystal growth, breaking of these symmetry rules is possible, which ultimately can lead to the presence of two different modifications in one single crystal [21].

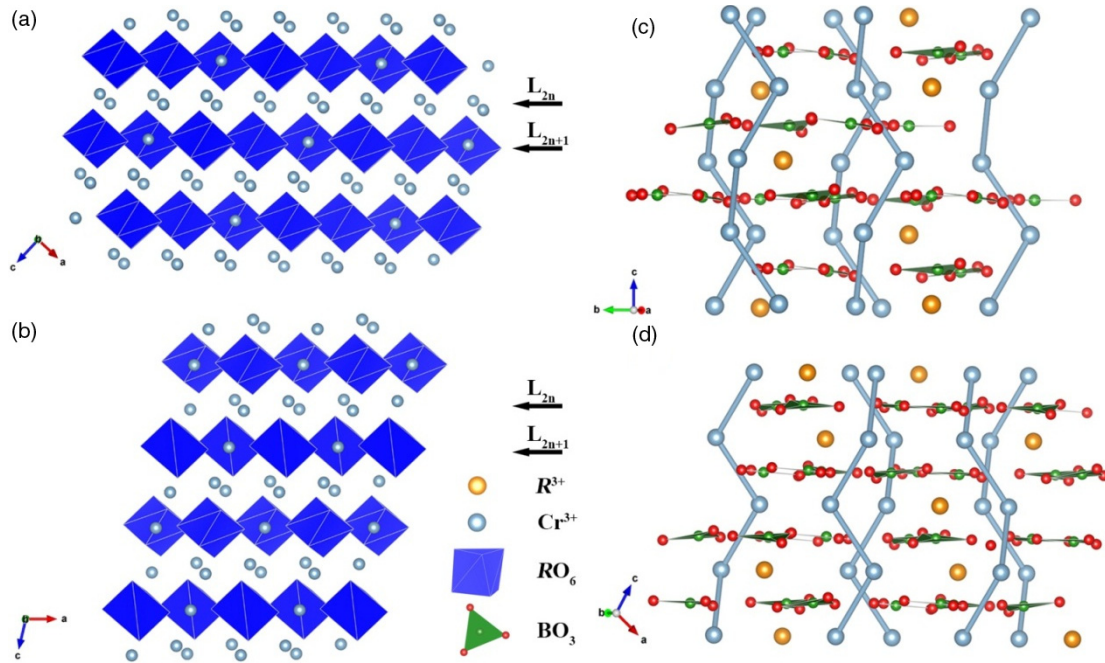


FIG. 1. Crystal structure of the (a)  $R32$  and (b)  $C2/c$  modifications of rare earth (RE) chromium borates  $RCr_3(BO_3)_4$ .  $L_{2n}$  layers consist of the  $CrO_6$  octahedra, but  $L_{2n+1}$  layers include both the  $RO_6$  prisms and  $CrO_6$  octahedra. Blue balls connected by rods represent chains of the  $Cr^{3+}$  ions running along the  $c$  axis in both (a)  $R32$  and (b)  $C2/c$  phases.

In both modifications, helical chains of magnetic  $Cr^{3+}$  ions interconnected by  $BO_3$  triangles and isolated  $SmO_6$  prisms are present. The distance between the nearest-neighbor ( $nn$ )  $Cr^{3+}$  ions within a chain  $R_{nn}$  is significantly less than distances between the two next-nearest- ( $nnn$ ) and the four next-next-nearest-neighbor ( $nnnn$ )  $Cr^{3+}$  ions belonging to different chains  $R_{nnn}$  and  $R_{nnnn}$ , respectively (in the  $R32$  phase,  $R_{nn} = 0.308$  nm,  $R_{nnn} = 0.443$  nm, and  $R_{nnnn} = 0.483$  nm), and therefore quasi-one-dimensional magnetic properties are anticipated. However, the presence of the inversion center in the  $C2/c$  structure cancels nonlinear optical and magnetoelectric properties. For the interpretation of the optical spectra, it is essential to know the local symmetries of the RE and chromium sites. In both phases, the  $Sm^{3+}$  ions occupy a single position with the  $D_3$  ( $C_2$ ) point symmetry group in the case of the  $R32$  ( $C2/c$ ) structure. While the  $Cr^{3+}$  ions are in a single  $C_2$  symmetry position in the  $R32$  phase, there are two different chromium sites with the  $C_2$  and  $C_1$  symmetry in the  $C2/c$  structure.

#### IV. EXPERIMENTAL RESULTS AND DISCUSSION

##### A. Spectroscopic evidence for the presence of both $R32$ and $C2/c$ phases in one single crystal

First, we have checked the phase composition of the obtained crystals. As both modifications ( $R32$  and  $C2/c$ ) are extremely close in their structure, it is difficult to identify them by powder diffraction patterns. Following Refs. [21,22], we applied the method of vibrational spectroscopy. Figure 2(a) displays the FIR spectra of  $SmCr_3(BO_3)_4$  powder at different temperatures. This spectral region corresponds to external vibrations; internal vibrations of closely bound  $BO_3$  groups

lie  $>500$   $cm^{-1}$ . A comparison of the observed modes with the data on earlier thoroughly studied iron borates with the  $R32$  structure [32] shows that the weak lines with frequencies (at 240 K) 185, 221, 248, 301, 308, 322, and 336  $cm^{-1}$  belong to the monoclinic  $C2/c$  phase.

The question arises whether there are different crystals in different phases or both phases can coexist in one crystal. As it has been shown earlier [33], the  $^4I_{9/2} \rightarrow ^4F_{3/2}$  optical transition of the  $Nd^{3+}$  impurity in RE chromium borates can serve as a sensitive spectroscopic probe of a phase composition. In a single-phase paramagnetic material, this transition should consist of two lines. Figure 2(b) shows the absorption spectrum of a  $SmCr_3(BO_3)_4:Nd$  (1 at. %) single crystal in a paramagnetic phase. Three lines are present in the spectrum. The low-frequency doublet can be unambiguously identified with the transition in the  $R32$  and  $C2/c$  phases, based on the results on the solid solutions  $Nd_xGd_{1-x}Cr_3(BO_3)_4$  [33]. It should be noted that the relative intensities of components of the doublet are not proportional to the relative quantities of the two phases because of enhancement of the forced electric dipole (ED) transitions and relaxation of the selection rules at the symmetry lowering from  $D_3$  to  $C_2$ . The spectra of the  $Sm^{3+}$  ions in  $SmCr_3(BO_3)_4$  crystals are well interpreted in the frame of the  $D_3$  point symmetry group, i.e., the  $R32$  phase (see Sec. IV E); however, in some spectral multiplets, extra lines are observed, testifying the presence of another phase.

##### B. Calorimetry

The temperature dependence of the heat capacity of  $SmCr_3(BO_3)_4$  is shown in Fig. 3. There are no anomalies between 300 and 10 K, which indicates the absence of phase transitions in this temperature range. However,  $<10$  K, three

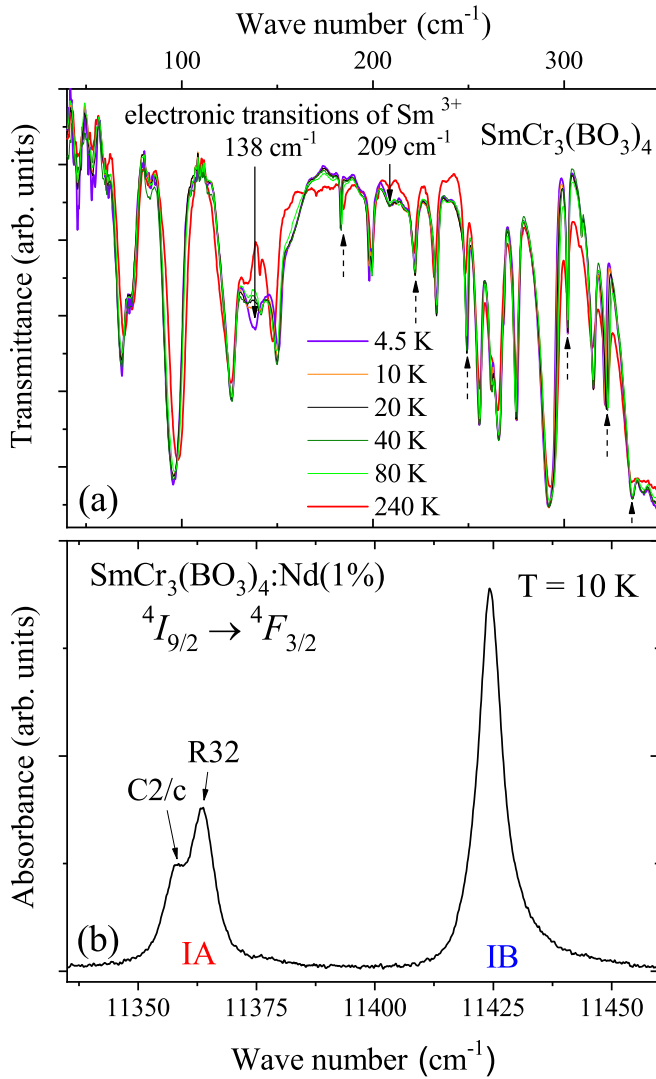


FIG. 2. Signatures of the monoclinic phase in the (a) vibrational far-infrared (FIR) spectra of a  $\text{SmCr}_3(\text{BO}_3)_4$  powder sample and (b) spectrum of the  ${}^4I_{9/2} \rightarrow {}^4F_{3/2}$  optical transition of the  $\text{Nd}^{3+}$  probe in a paramagnetic  $\text{SmCr}_3(\text{BO}_3)_4:\text{Nd}$  (1 at. %) single crystal. In (a), vibrational modes of the  $C2/c$  phase are shown by upward arrows.

maxima are observed in the heat capacity, as the inset of Fig. 3 clearly demonstrates. The low-temperature maximum at  $T_3 = 4.3$  K has a qualitatively different shape than those appearing at  $T_{N1}$  and  $T_{N2}$ . It is more symmetric and narrower, which suggests that it can be related to a first-order phase transition. The temperature dependence of the heat capacity near temperatures  $T_{N1} = 7.8$  K and  $T_{N2} = 6.7$  K is characteristic of second-order phase transitions.

The three maxima reside on a broad low-temperature anomaly (note that, at low temperatures, the phonon contribution to the specific heat is small and has no anomalies, and the lattice specific heat uniformly tends to zero as  $T \rightarrow 0$ ). For compounds with RE ions, the so-called Schottky contribution to the specific heat is well known, which leads to a wide maximum; it occurs due to the depopulation of excited energy levels of a RE ion. The CF levels of the ground  ${}^6H_{5/2}$  multiplet of  $\text{Sm}^{3+}$  in  $\text{SmCr}_3(\text{BO}_3)_4$  have the energies 0, 138, and

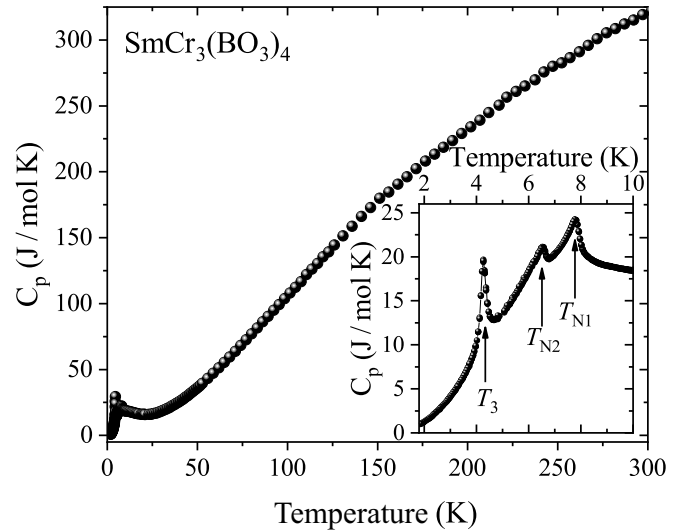


FIG. 3. Temperature dependence of the heat capacity of a  $\text{SmCr}_3(\text{BO}_3)_4$  single crystal. The inset shows the low-temperature part of the dependence on an enlarged scale; phase transitions are indicated by arrows.

$209 \text{ cm}^{-1}$ , but the ground-state exchange splitting does not exceed  $4 \text{ cm}^{-1}$  at 3.5 K (see Sec. IV E). Our estimates show that the latter gives a Schottky contribution peak  $< 2.5$  K, whereas subsequent CF levels contribute  $> 80$  K [23]. Thus, the excited energy levels of  $\text{Sm}^{3+}$  cannot explain the observed broad anomaly in  $\text{SmCr}_3(\text{BO}_3)_4$ . Possibly, it relates to low dimensionality of the chromium magnetic subsystem.

### C. Magnetic measurements on $\text{SmCr}_3(\text{BO}_3)_4$

Figure 4 shows the temperature dependences of the magnetic susceptibility of a  $\text{SmCr}_3(\text{BO}_3)_4$  single crystal in a magnetic field  $B = 0.1$  T along the crystallographic directions  $b^*[\chi_{\perp}(T)]$  and  $c[\chi_{\parallel}(T)]$ . At sufficiently high temperatures ( $\geq 35$  K), the susceptibilities  $\chi_{\perp}$  and  $\chi_{\parallel}$  coincide and obey the Curie-Weiss law with the Weiss temperature  $\Theta \approx -18$  K and the value of the effective magnetic moment  $\mu_{\text{eff}} = 6.8 \mu_B$ .

The negative value of the Weiss temperature indicates the dominance of the antiferromagnetic exchange interaction and the formation of an antiferromagnetic structure at magnetic ordering. The value of the effective moment is consistent with the presence of two magnetic subsystems, those of the  $\text{Cr}^{3+}$  and  $\text{Sm}^{3+}$  ions. The corresponding  $g$  factors and angular moments are  $g_{\text{Cr}} = 2$  and  $S_{\text{Cr}} = \frac{3}{2}$  for the  $\text{Cr}^{3+}$  ion (the ground state of chromium ions is an orbital singlet) and  $g_{\text{Sm}} = \frac{2}{7}$  and  $J_{\text{Sm}} = \frac{5}{2}$  for the  $\text{Sm}^{3+}$  ion. Neglecting the interaction of magnetic subsystems, we obtain the effective magnetic moment for the entire system  $\mu_{\text{eff}} = [3\mu_{\text{eff}}(\text{Cr}^{3+})^2 + \mu_{\text{eff}}(\text{Sm}^{3+})^2]^{1/2} \approx 6.76 \mu_B$ . The deviation of the temperature dependence of the susceptibility from the Curie-Weiss law long before the phase transitions in  $\text{SmCr}_3(\text{BO}_3)_4$  (starting from  $\sim 40$  K), the same as in the case of  $\text{NdCr}_3(\text{BO}_3)_4$  [23], and a broad maximum at  $T \sim 13$  K evidence a low dimensionality of the chromium magnetic subsystem.



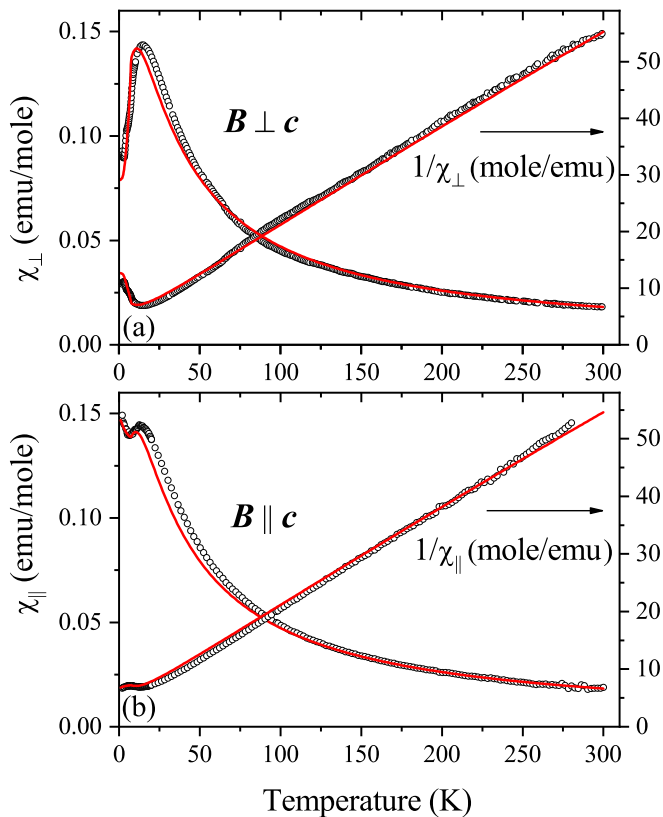


FIG. 4. Measured (symbols) and calculated (red lines) temperature dependences of the dc magnetic susceptibility in magnetic fields (a)  $\mathbf{B} \perp c$  and (b)  $\mathbf{B} \parallel c$  for  $B = 0.1$  T.

The anisotropy of the magnetic susceptibility along ( $\chi_{\parallel}$ ) and perpendicular ( $\chi_{\perp}$ ) to the  $c$  axis ( $\chi_{\parallel} > \chi_{\perp}$ ) begins to manifest itself when approaching the maximum of the susceptibility from the side of high temperatures and increases with a further decrease in temperature. The low-temperature behavior of the susceptibilities as well as their change in an applied magnetic field up to 5 T are shown in more detail in Fig. 5.

A noticeable decrease in the susceptibility  $\chi_{\perp}$  at low temperatures and a significantly weaker change in the susceptibility  $\chi_{\parallel}$  indicate that, in the antiferromagnetic state, the magnetic moments lie in the basal plane. Anomalies at the Néel point  $T_{N1} = 7.8$  K and at  $T_{N2} \sim 6.7$  K in the temperature dependences of the susceptibilities are very weak. However, one can clearly see sharp changes in the susceptibilities at the phase transition at  $T_3 \sim 4.3$  K. With an increase in the magnetic field, the character of the temperature dependences of the susceptibilities undergoes changes, especially significant for measurements along the  $b^*$  axis, where a decrease in  $\chi_{\perp}$  is replaced by an increase below  $T_3$  in a field of 5 T, but in the region of 4 K, a slight abrupt decrease in  $\chi_{\perp}$  is observed.

#### Magnetization

Figure 6 presents the field dependences of the magnetization  $M(B)$ , measured along the  $c$  and  $b^*$  axes in the paramagnetic phase. While in the case of  $\mathbf{B} \parallel c$  the  $M(B)$  dependence is linear in both paramagnetic and magnetically

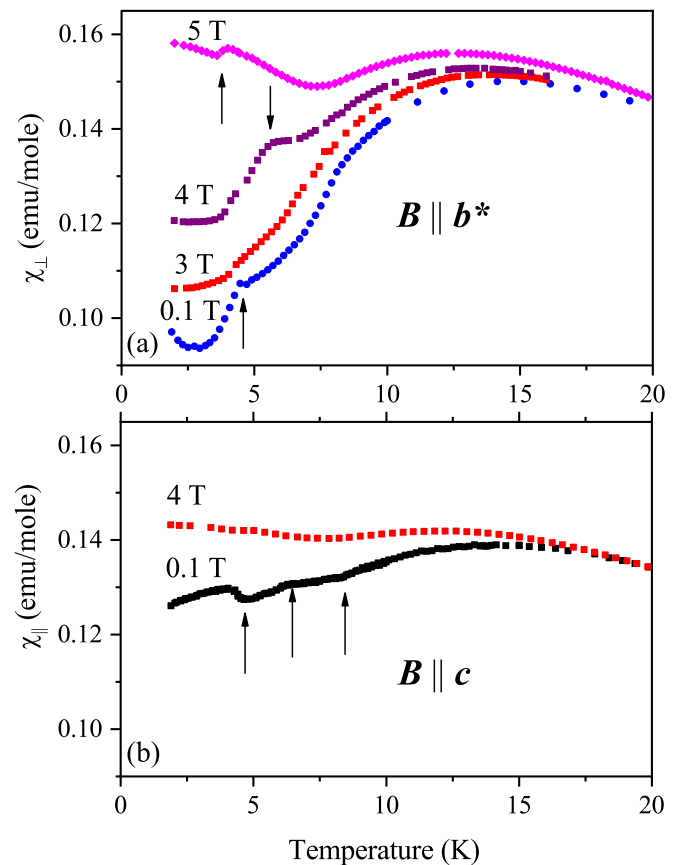


FIG. 5. Temperature dependences of the low-temperature dc susceptibility  $\chi = M/B$  measured in different magnetic fields for two crystallographic directions: (a)  $\mathbf{B} \parallel b^*$  and (b)  $\mathbf{B} \parallel c$ . Arrows indicate positions of the anomalies on the  $\chi(T)$  dependences.

ordered (not shown) phases, for  $\mathbf{B} \parallel b^*$ , the  $M(B)$  dependence, linear in a paramagnetic phase, becomes nonlinear in a magnetically ordered phase and undergoes a rather sharp increase in fields of  $\sim 4$ – $4.5$  T (Fig. 7), which manifests itself as a peak in the  $dM/dB$  derivatives (inset of Fig. 7). Herewith, the magnetization reaches approximately the same values as along the  $c$  axis. The different character of magnetization curves at low temperatures for  $\mathbf{B} \parallel c$  and  $\mathbf{B} \perp c$  in the ordered state at 2 K is illustrated in the bottom insert of Fig. 7.

Based on the obtained data, it is possible to make some assumptions about the nature of the magnetic ordering in  $\text{SmCr}_3(\text{BO}_3)_4$ . At  $T < T_{N1}$ , an antiferromagnetic ordering of the easy-plane type most likely appears. A very weak manifestation of anomalies in the magnetic characteristics at  $T = T_{N2}$  suggests, in accordance with studies on non-single-phase chromium borates of lanthanum and dysprosium [28,29], that  $T_{N2}$  corresponds to the Néel temperature of the impurity monoclinic phase  $C2/c$ . The nature of the transition at  $T_3$  is not clear. This cannot be a spin reorientation of chromium ions to the  $c$  axis since such a reorientation would cause a significant increase in  $\chi_{\perp}$  and a decrease in  $\chi_{\parallel}$ , which is not the case experimentally. It is possible that, at  $T < T_3$ , a spiral structure appears in the basal plane, as in neodymium iron borate at low temperatures [34], or some noncollinear (triangular) structure. Note that additional features in the temperature dependences

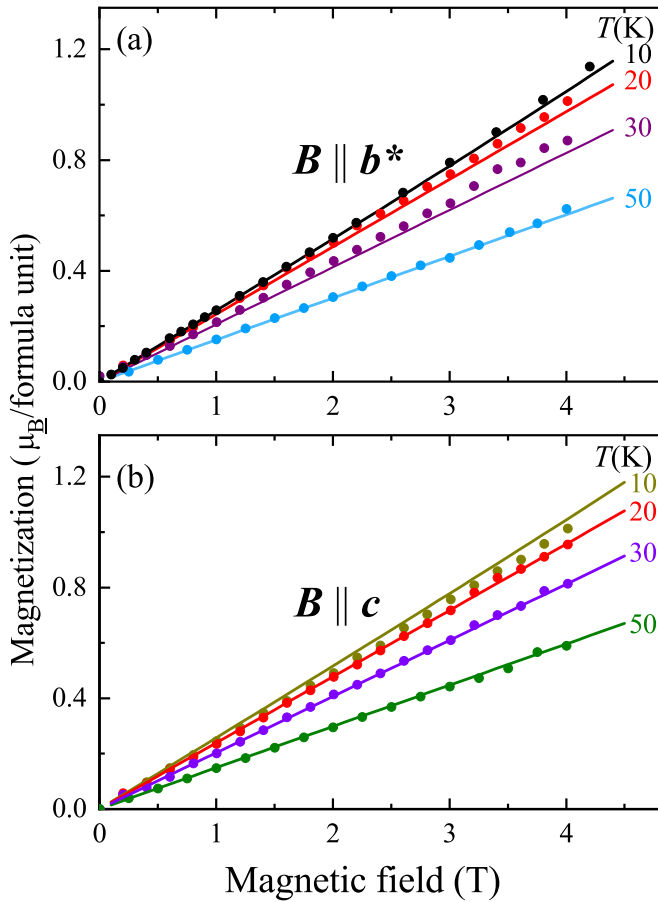


FIG. 6. Measured (symbols) and calculated (solid lines) field dependences of magnetization at different temperatures in magnetic fields (a)  $\mathbf{B} \perp c$  and (b)  $\mathbf{B} \parallel c$ .

of the magnetic susceptibility below the Néel temperature, the nature of which remained unclear, were also observed for  $\text{EuCr}_3(\text{BO}_3)_4$  [25].

The nature of the nonlinear increase in magnetization along the  $b^*$  axis in fields of  $\sim 4$ – $4.5$  T also remains not fully understood. The observed increase in magnetization is not too sharp and rather resembles a gradual rotation of the iron spins in easy-plane iron borates to a direction perpendicular to the field than transitions of the spin-flop type. However, in iron borates, this transition was observed in significantly lower fields ( $< 1$  T). In several other chromium borates, the field dependences of magnetization at low temperatures also exhibit some features, the nature of which remains unclear. For example, in  $\text{NdCr}_3(\text{BO}_3)_4$ , in fields of  $\sim 3$  T at  $T = 2$  K, an increase in the slope of the  $M(B)$  curve was observed [23]. A metamagnetic transition at  $T = 1.9$  K in a field  $B_{\text{cr}} = 4.7$  T was observed in  $\text{EuCr}_3(\text{BO}_3)_4$  [25]. Finally, an abrupt increase in magnetization was recently recorded in  $\text{GdCr}_3(\text{BO}_3)_4$  at low temperatures in fields of  $\sim 3.9$ – $4.2$  T, which the authors attributed to the reorientation of the gadolinium magnetic moments along the magnetic field [26]. However, such an interpretation of the observed transition is questionable based on the magnetization values before the transition ( $\sim 9 \mu_{\text{B}}/\text{f.u.}$ ) and after the transition ( $\sim 11 \mu_{\text{B}}/\text{f.u.}$ ). In contrast to  $\text{GdCr}_3(\text{BO}_3)_4$ , in which the

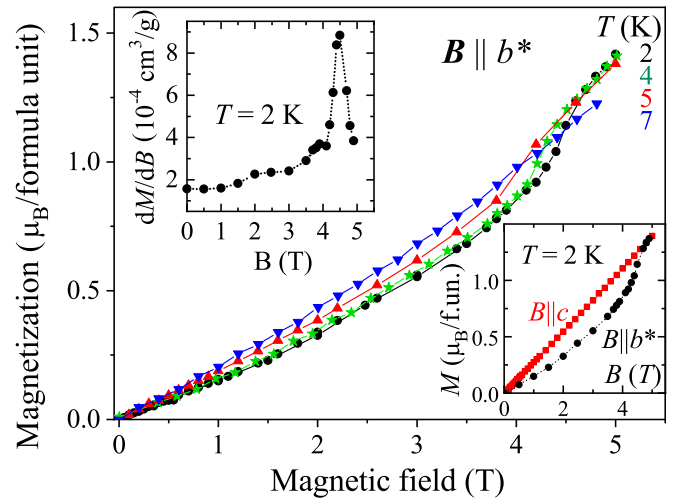


FIG. 7. Measured (symbols) field dependences of magnetization at different temperatures in a magnetic field  $\mathbf{B} \parallel b^*$ . Insets: (top) derivative  $dM/dB$  at  $T = 2$  K and (bottom) comparison of magnetization along and perpendicular to the  $c$  axis at  $T = 2$  K.

transition was observed for all crystallographic directions, it was not found in  $\text{SmCr}_3(\text{BO}_3)_4$  at  $\mathbf{B} \parallel c$ .

As follows from Figs. 5(a) and 7, in magnetic fields greater than the critical one, the value of the susceptibility is restored to a value in the region of the Néel temperature, i.e., it can be assumed that the vectors of antiferromagnetism have turned toward the direction perpendicular to the magnetic field. At the same time, the anomaly in the  $\chi_{\perp}(T)$  curve at  $T = T_3$  persists in the field  $B = 5$  T  $> B_{\text{cr}}$  [Fig. 5(a)]. This indicates that the transitions in temperature at  $T_3$  and in field at  $B_{\text{cr}}$  are not related to each other.

Figure 8 shows a sketch of the  $B$ - $T$  phase diagram of  $\text{SmCr}_3(\text{BO}_3)_4$  according to the data of measurements of the temperature and field dependences of magnetization as well as magnetoelectric characteristics (see below). It should be noted that this is an approximate diagram. Anomalies were observed on the temperature dependences of dc susceptibility not in all fields at all three temperatures of phase transitions. The uncertainty of temperature is  $\sim 0.3$  K, and the uncertainty of field is  $\sim 0.5$  T. The above-noted independence of the transitions on field and on temperature is reflected by the intersection of the lines  $B_{\text{cr}}(T)$  and  $T_3(B)$ . It can be assumed that the  $B_{\text{cr}}(T)$  curve goes to  $T_{\text{N}1}(B)$  since, despite significant expanding of the related anomalies in the magnetization curves with increasing temperature, they persist up to  $7$  K  $> T_{\text{N}2}$ .

Thus, based on the available data, it is possible to draw so far rather general preliminary conclusions about the nature of the magnetic structure of  $\text{SmCr}_3(\text{BO}_3)_4$  below the Néel point, that the spins are oriented mainly in the basal plane. As for the nature of the observed low-temperature spontaneous transition at  $T_3$  and the transition induced by the magnetic field  $\mathbf{B} \parallel b^*$ , its elucidation requires additional research.

#### D. Magnetolectric effect in $\text{SmCr}_3(\text{BO}_3)_4$

In Ref. [26], a magnetic-field-induced electric polarization in  $\text{GdCr}_3(\text{BO}_3)_4$  was demonstrated, and in Ref. [27], its existence was declared for the easy-plane phase of  $\text{TbCr}_3(\text{BO}_3)_4$ ,

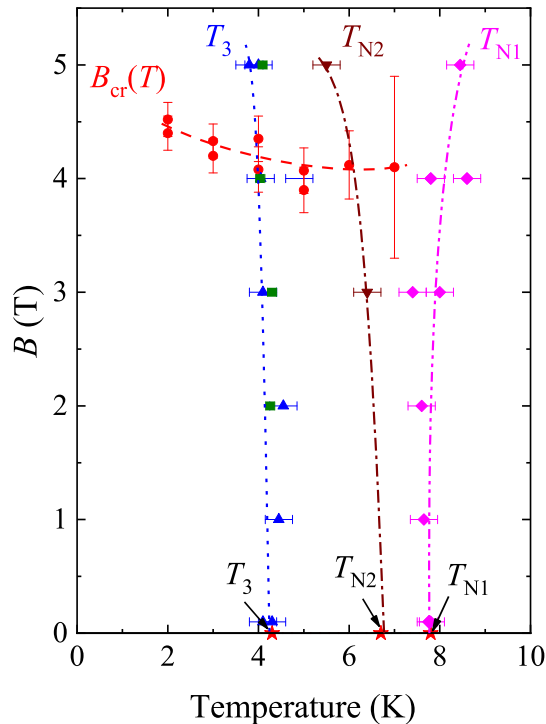


FIG. 8. Sketch of the  $B$ - $T$  phase diagram of  $\text{SmCr}_3(\text{BO}_3)_4$  based on measurements of temperature dependences of the heat capacity (red stars), magnetization (blue, magenta, and brown symbols), and electric charge change (olive squares), as well as field dependences of magnetization (red circles). Double points at the same values of temperature or field correspond to measurements on different crystals (samples).

which gave grounds to classify these chromium borates as magnetoelectrics. We also searched for magnetoelectric properties in a mosaic sample made up of many small  $\text{SmCr}_3(\text{BO}_3)_4$  oriented crystals in the  $P_a(\mathbf{B} \perp c)$  geometry (see Sec. II). Some anomalies were found in both the field and temperature dependences of the charge. However, since the field dependences were not reliable enough and reproducible, we do not present them here. On the other hand, on the temperature dependences, the character of the anomaly at the phase transition at  $T_3$  is well reproduced in different magnetic fields from 2 to 5 T (see Fig. 9). With an increase in temperature in the region of 4.0–4.35 K, a sharp burst of charge occurs, and its value after the completion of the transition becomes greater than it was below the transition. Some features near  $T_3$  are observed also at  $B = 0$  and 1 T, but they are not so expressive. No clear anomalies were found at the Néel point  $T_{N1}$  and at  $T = T_{N2}$ , from which it can be assumed that spontaneous electric polarization most likely appears at  $T_3$ .

To estimate the magnitude of the polarization, it is necessary to know the total surface area of the crystals. However, this is not enough either. As is known, in noncentrosymmetric crystals, which include trigonal crystals of the  $R32$  group, the polarization sign is determined by the chirality and the true direction (+ or – sign) of the crystallographic axes. Obviously, even if all crystals have the same chirality, we cannot know the true directions of the axes of each crystal and

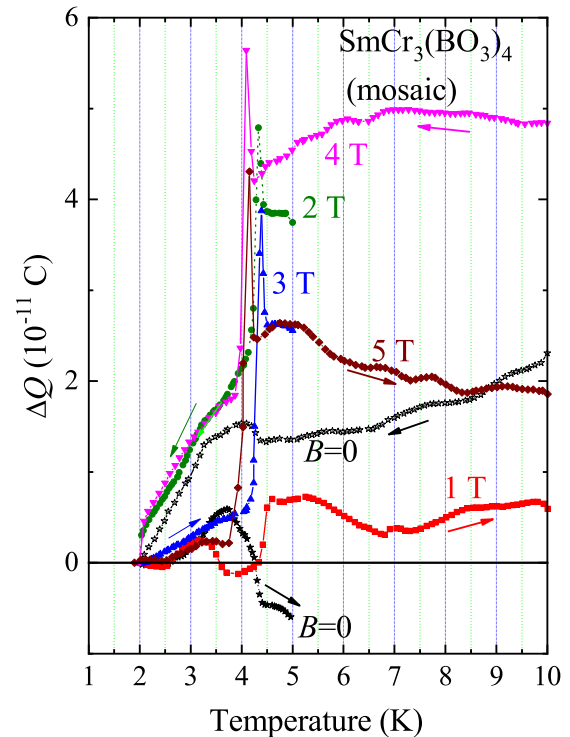


FIG. 9. Temperature dependences of the change in the electric charge of the  $a$ -cut mosaic in different magnetic fields in the basal plane. The charge at  $T = 2$  K is taken as the reference point. Arrows indicate the directions of the temperature sweep.

lay the mosaic in the correct way. Therefore, the difference signal from crystals with polarization conventionally upward and crystals with downward polarization is measured. This is also supported by the presence of a burst and not just a jump: the polarization of not all crystals is switched simultaneously, and there is a certain competition of contributions. Another possible explanation of such complex anomaly in the charge behavior at  $T_3$  could also be related to a piezoelectric contribution at the first-order phase transition at  $T_3$  in the noncentrosymmetric crystal.

Other peculiarities in the temperature dependences are associated, in addition to a constant time drift, with an inevitable flow of charge in the circuit when the temperature changes. This is manifested in the different behavior of the curves  $\Delta Q(T)$  in the heating and cooling mode at  $B = 0$ . On the other hand, the positions of the transition temperature  $T_3$  remain very close to each other. Thus, despite a difference in values of the upward and downward  $\Delta Q(T)$  branches, their temperature hysteresis at the transition is small ( $\sim 0.05$ – $0.08$  K), which even allows us to estimate the shift of the  $T_3(B)$  line in the field shown in Fig. 8.

## E. Optical spectroscopy

### 1. Spectra of paramagnetic $\text{SmCr}_3(\text{BO}_3)_4$ : CF levels of $\text{Sm}^{3+}$

Figure 10 shows the transmission spectrum of a paramagnetic  $\text{SmCr}_3(\text{BO}_3)_4$  single crystal at 270 K over the entire spectral region under study. The spectrum contains narrow

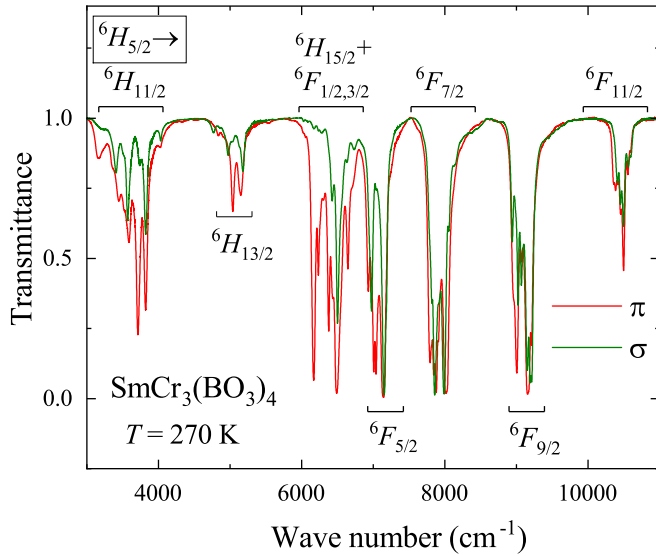


FIG. 10. Transmission spectrum of a  $\text{SmCr}_3(\text{BO}_3)_4$  crystal at a temperature of 270 K in  $\pi$  (red curve) and  $\sigma$  (green curve) polarizations. The final states for optical transitions from the sublevels of the ground  ${}^6H_{5/2}$  multiplet of  $\text{Sm}^{3+}$  ions are indicated.

lines corresponding to  $f$ - $f$  optical transitions between the energy levels of the  $4f^5$  electronic shell of the  $\text{Sm}^{3+}$  ion.

In a CF of any symmetry lower than a cubic one, each  $2S+1L_J$  multiplet of a free Kramers ion (i.e., the ion with an odd number of electrons, like  $\text{Sm}^{3+}$ ) splits into  $(2J+1)/2$  Kramers doublets which transform according to the two-valued irreducible representations  $\Gamma_4$  and  $\Gamma_{56}$  in the case of the  $D_3$  point symmetry group (the  $R32$  phase) or  $\Gamma_{34}$  in the case of the  $C_2$  group (the  $C2/c$  phase). Selection rules for the ED and magnetic-dipole (MD) optical transitions in the former case are presented in Table I. While both  $\sigma$ - and  $\pi$ -polarized ED and MD  $\Gamma_4 \rightarrow \Gamma_4$  transitions are allowed, selection rules for the  $\Gamma_4 \rightarrow \Gamma_{56}$  and  $\Gamma_{56} \rightarrow \Gamma_{56}$  transitions are polarization sensitive (see Table I). The selection rules relax for the  $C_2$  point group, where all transitions are allowed.

At a sufficiently low temperature, when excited CF levels of the ground  ${}^6H_{5/2}$  multiplet are not populated, the observed spectral lines reflect the Stark structure of the excited multiplets. Figure 11 shows the absorption spectrum of paramagnetic  $\text{SmCr}_3(\text{BO}_3)_4$  at  $T = 15 \text{ K} > T_{N1}$  in the region of the  ${}^6H_{5/2} \rightarrow {}^6H_{13/2}$  transition of the  $\text{Sm}^{3+}$  ion in two different polarizations. It is worth noting that usually MD transitions have a negligible intensity, with an exception of transitions

TABLE I. Allowed transitions between the CF energy levels of a Kramers ion in a position with the  $D_3$  point symmetry group.  $d_i$  and  $\mu_i$ ,  $i = x, y, z$ , denote components of the ED and MD moments, respectively.

	$\Gamma_4$	$\Gamma_{56}$
$\Gamma_4$	$d_x, d_y, d_z; \mu_x, \mu_y, \mu_z$ $\sigma, \pi$ ED; $\sigma, \pi$ MD	$d_x, d_y; \mu_x, \mu_y$ $\sigma$ ED; $\pi$ MD
$\Gamma_{56}$	$d_x, d_y; \mu_x, \mu_y$ $\alpha, \sigma$ ED; $\alpha, \pi$ MD	$d_z, \mu_z$ $\pi$ ED; $\sigma$ MD

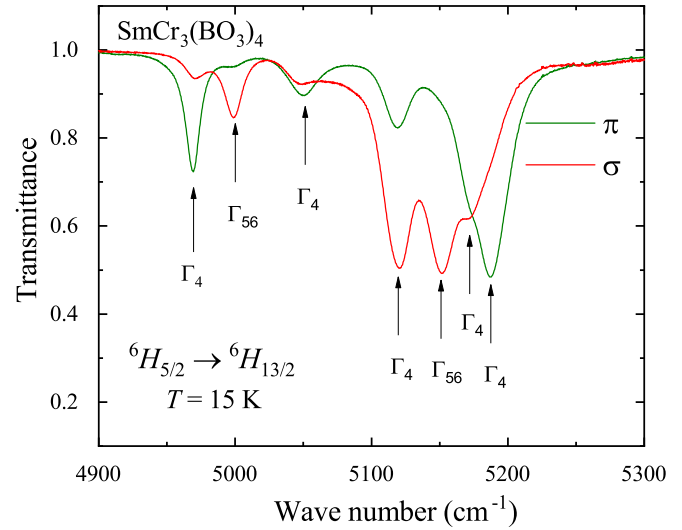


FIG. 11. Transmission spectrum of  $\text{SmCr}_3(\text{BO}_3)_4$  in the region of the  ${}^6H_{5/2} \rightarrow {}^6H_{13/2}$  transition in the  $\text{Sm}^{3+}$  ion at a temperature  $T = 15 \text{ K} > T_{N1}$  in the  $\sigma$  and  $\pi$  polarizations.

allowed in a free ion (i.e., the  ${}^6H_{5/2} \rightarrow {}^6H_{7/2}$  transition of  $\text{Sm}^{3+}$ ). The CF multiplet  ${}^6H_{13/2}$  contains five  $\Gamma_4$  levels and two  $\Gamma_{56}$  levels for  $\text{Sm}^{3+}$  in the  $D_3$  symmetry positions. Consulting the selection rules for ED transitions, we find that, in the case of the  $\Gamma_4(\Gamma_{56})$  symmetry of the ground state, two (five) transitions in  $\pi$  polarization are forbidden, while the other five (two) lines can be observed in both  $\pi$  and  $\sigma$  polarizations. The experimentally observed spectrum (Fig. 11) corresponds to the  $\Gamma_4$  symmetry of the ground state. Guided by the selection rules, we find irreducible representations that determine the symmetry properties of the wave functions of the CF levels of the  ${}^6H_{13/2}$  multiplet. They are shown in Fig. 11 and Table II (next to the found energies of the CF levels). Having performed a similar analysis of other optical multiplets, we obtained the data presented in the first column of Table II.

It should be noted that the spectra of a given  $\text{SmCr}_3(\text{BO}_3)_4$  crystal could be well interpreted in the frame of a single  $R32$  structural phase. The  $C2/c$  phase, possibly, in the  ${}^6H_{5/2} \rightarrow {}^6H_{13/2}$  spectra manifests itself by weak  $\pi$ -polarized lines at 4997 and 5152  $\text{cm}^{-1}$ . These lines are totally absent in the spectra of  $\text{SmFe}_3(\text{BO}_3)_4$  crystals having the  $R32$  structure, which excludes their MD nature.

To find the CF structure of the ground multiplet, knowledge of which is necessary for interpreting the magnetic and thermodynamic properties of  $\text{SmCr}_3(\text{BO}_3)_4$ , the temperature-dependent spectra were studied. Figure 12 shows the transmission spectra in the region of the  ${}^6H_{5/2} \rightarrow {}^6F_{5/2}$  transition in the  $\sigma$  and  $\pi$  polarizations at  $T > T_{N1}$  (20–200 K). With decreasing temperature, the intensity of spectral lines corresponding to transitions from excited CF levels of the ground  ${}^6H_{5/2}$  multiplet decreases due to a decrease in the populations of these levels with temperature.

Analyzing the temperature dependences of the intensities of the “freezing” absorption lines and considering the distances to the main spectral lines, we determined the energies of the CF levels of the ground  ${}^6H_{5/2}$  multiplet: 0, 138,



TABLE II. Energy levels and  $g$  factors of the  $\text{Sm}^{3+}$  ion in the paramagnetic  $R32$  phase of  $\text{SmM}_3(\text{BO}_3)_4$ ,  $M = \text{Cr, Fe}$ .

$2S+1L_J$	$\text{SmCr}_3(\text{BO}_3)_4$		$\text{SmFe}_3(\text{BO}_3)_4$	$\text{SmCr}_3(\text{BO}_3)_4$	
	Exper.	Theor.	Exper. [35]	$g_{\parallel}$	$g_{\perp}$
${}^6H_{5/2} \Gamma_4 \text{ I}$	0	0	0	0.496	0.649
$\Gamma_{56} \text{ II}$	138.3	137.1	135	1.625	0
$\Gamma_4 \text{ III}$	209.4	208.9	220	1.417	0.012
${}^6H_{7/2} \Gamma_4 \text{ A}$	—	1085.8	1091	1.132	1.864
$\Gamma_4 \text{ B}$	—	1121.8	1115	1.742	0.110
$\Gamma_{56} \text{ C}$	—	1179.6	1173	2.328	0
$\Gamma_4 \text{ D}$	—	1280.3	—	4.961	0.943
${}^6H_{9/2} \Gamma_4 \text{ A}$	—	2299.5	2296	3.202	2.941
$\Gamma_4 \text{ B}$	—	2322.8	2321	0.651	2.076
$\Gamma_{56} \text{ C}$	—	2351.7	—	2.931	0
$\Gamma_4 \text{ D}$	—	2399.3	2404	0.574	4.211
$\Gamma_{56} \text{ E}$	—	2491.4	2509	9.205	0
${}^6H_{11/2} \Gamma_4 \text{ A}$	3607.8	3610.1	—	1.094	6.992
$\Gamma_{56} \text{ B}$	—	3644.3	—	1.939	0
$\Gamma_4 \text{ C}$	3658.7	3664.7	—	0.739	6.087
$\Gamma_{56} \text{ D}$	3711	3709.5	3716	9.027	0
$\Gamma_4 \text{ E}$	3733.3	3726.7	3729	3.244	6.012
$\Gamma_4 \text{ F}$	3822	3809.3	3835	12.94	0.036
${}^6H_{13/2} \Gamma_4 \text{ A}$	4969.4	4969.5	4964	1.227	8.766
$\Gamma_{56} \text{ B}$	4996.6	5001	4994	3.740	0
$\Gamma_4 \text{ C}$	5052.4	5055.9	5055	5.711	3.202
$\Gamma_4 \text{ D}$	5119	5118.1	5119	8.175	3.099
$\Gamma_{56} \text{ E}$	5152	5151.7	5152	11.30	0
$\Gamma_4 \text{ F}$	5172.1	5170.8	5178	10.83	2.747
$\Gamma_4 \text{ G}$	5187.4	5174.3	5203	13.21	2.825
${}^6H_{15/2} \Gamma_4 \text{ A}$	—	6334.5	6333	0.947	10.24
$\Gamma_{56} \text{ B}$	6373	6372.4	—	4.341	0
$\Gamma_4 \text{ C}$	6443.9	6440	—	5.201	2.988
$\Gamma_{56} \text{ D}$	6513.1	6516.3	6518	18.76	0
$\Gamma_4 \text{ E}$	6531.9	6532.1	6543	8.064	2.812
$\Gamma_{56} \text{ F}$	6625.7	6639.3	—	9.499	0
$\Gamma_4 \text{ G}$	6725.1	6716.2	—	13.58	1.298
$\Gamma_4 \text{ H}$	6742.8	6735.2	—	16.22	1.218
${}^6F_{1/2} \Gamma_4$	—	6381.8	6372	1.277	0.392
${}^6F_{3/2} \Gamma_4 \text{ A}$	6640.4	6640.5	6626	1.210	2.830
$\Gamma_{56} \text{ B}$	6653	6662.4	6649	5.349	0
${}^6F_{5/2} \Gamma_{56} \text{ A}$	7133	7128.5	7133	3.883	0
$\Gamma_4 \text{ B}$	7144.8	7155.7	7148	4.081	1.062
$\Gamma_4 \text{ C}$	7177	7192	7174	0.446	3.140
${}^6F_{7/2} \Gamma_4 \text{ A}$	7982	7976.9	7982	4.031	2.860
$\Gamma_{56} \text{ B}$	7996.7	8003.4	8000	4.389	0
$\Gamma_4 \text{ C}$	8018.4	8023.5	8021	5.479	2.118
$\Gamma_4 \text{ D}$	8052	8075.4	8052	2.871	4.875
${}^6F_{9/2} \Gamma_4 \text{ A}$	9142.3	9143.2	9146	8.741	2.458
$\Gamma_{56} \text{ B}$	9159.6	9173.6	9158	11.21	0
$\Gamma_4 \text{ C}$	9185.1	9190.1	9191	4.688	3.177
$\Gamma_{56} \text{ D}$	9211	9219.8	9211	3.891	0
$\Gamma_4 \text{ E}$	—	9224.9	9213	0.111	6.430
${}^6F_{11/2} \Gamma_4 \text{ A}$	10489	10486	10489	15.75	0.012
$\Gamma_4 \text{ B}$	10548	10559	10554	1.861	8.328
$\Gamma_{56} \text{ C}$	10562.1	10565	10565	7.627	0
$\Gamma_4 \text{ D}$	10589	10605	10589	5.906	3.088
$\Gamma_{56} \text{ E}$	10596.4	10610	10592	9.737	0
$\Gamma_4 \text{ F}$	10604.9	10619	10599	8.249	3.416

and  $209 \text{ cm}^{-1}$ , which coincide with the preliminary data of Ref. [30]. The positions of the saturated spectral lines IA, IB, and IC were determined from a comparison of the transmission spectra in the  $\sigma$  and  $\pi$  polarizations (Fig. 12). Direct transitions from the ground state to the excited CF levels of the ground  ${}^6H_{5/2}$  multiplet were observed in the FIR spectra of  $\text{SmCr}_3(\text{BO}_3)_4$  [see Fig. 2(a)].

It should be noted that the energies and symmetries of the CF levels of the  ${}^6H_J (J = \frac{5}{2}, \frac{11}{2}, \frac{13}{2}, \frac{15}{2})$  and  ${}^6F_J (J = \frac{1}{2}, \frac{3}{2}, \frac{5}{2}, \frac{7}{2}, \frac{9}{2}, \frac{11}{2})$  multiplets agree well with the corresponding spectral characteristics of  $\text{Sm}^{3+}$  ions in  $\text{SmFe}_3(\text{BO}_3)_4$  [35] (see Table II).

## 2. Spectra of $\text{Sm}^{3+}$ in $\text{SmCr}_3(\text{BO}_3)_4$ and of $\text{Er}^{3+}$ probe in $\text{SmCr}_3(\text{BO}_3)_4:\text{Er}$ below $T_{N1}$

Since  $\text{Sm}^{3+}$  is a Kramers ion, splitting of spectral lines should be observed at the magnetic ordering [23]. In the collinear easy-plane structure, for the  $R32$  phase, only the  $\Gamma_4$  energy levels split, including the ground state of the samarium ion (see Table II). Figure 13 shows the low-temperature absorption spectra in the region of the transition from the ground state of the  $\text{Sm}^{3+}$  ion to the CF level B ( $\Gamma_{56}$ ) of the  ${}^6H_{15/2}$  multiplet. In the absence of magnetic order, there is only one spectral line in this region at low temperatures. In an exchange field arising at the magnetic ordering, this line splits into two components due to the splitting of the ground state. The splitting of a relatively broad line becomes observable at  $\sim 7 \text{ K}$ , i.e., at  $T_{N2} < T < T_{N1}$ . The nature of the formation of a quasi-equidistant four-component structure with an interval of  $\sim 4 \text{ cm}^{-1}$  with a decrease in temperature below  $T_3 = 4.3 \text{ K}$  remains unclear due to the unknown magnetic structure of the low-temperature ( $T < T_3$ ) phase. We note, however, that the emerging spectral doublet of lower intensity at higher frequencies could be associated with the  ${}^6H_{5/2}(\Gamma_4 \text{ I}) \rightarrow {}^6F_{1/2}(\Gamma_4)$  transitions (see Table II).

We also studied the spectra of the  $\text{Er}^{3+}$  ion introduced as a probe into a  $\text{SmCr}_3(\text{BO}_3)_4$  single crystal. The temperature behavior of the IA line in the  ${}^4I_{15/2} \rightarrow {}^4I_{13/2}$  transition of  $\text{Er}^{3+}$  is shown in Fig. 14. Here, the line splitting is also observed explicitly at  $\sim 7 \text{ K}$  [see Fig. 14(a)]. To get some information on small splittings comparable with the linewidth, we analyzed the temperature shift of the center of gravity (COG) of the spectral lines shown in Figs. 13(a) and 14(a) using the formula  $v_{\text{COG}} = \sum_i v_i I_i / \sum_i I_i$ , where  $v_i$  is the frequency of the  $i$ th point, and  $I_i$  is the corresponding intensity. The results are presented in Figs. 13(b) and 14(b). Figure 14(b) also shows the temperature dependence of the linewidth. At  $T_{N1}$ , the temperature dependences of COG and the line width demonstrate an inflection point, more pronounced in the case of the Er-probe line. This can be interpreted in terms of a splitting of Kramers doublets, which persists into a paramagnetic phase due to short-range order but shows an inflection point when long-range order is established [36]. The most pronounced changes occur at the temperature  $T_3$ . A sharp shift in the position of the COG to the high-frequency region is observed [Figs. 13(b) and 14(b)]. In the case of the samarium line, this is because of emergence of new components at the high-frequency wing of the line [Fig. 13(a)]. In the case

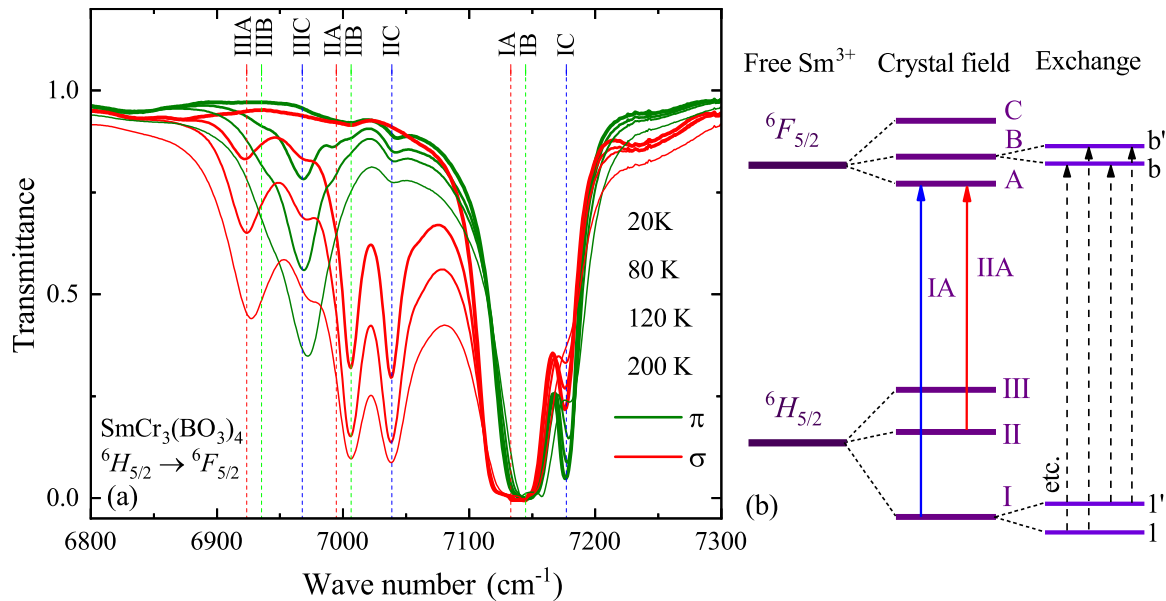


FIG. 12. (a) Transmission spectra of paramagnetic  $\text{SmCr}_3(\text{BO}_3)_4$  in  $\sigma$  and  $\pi$  polarizations at different temperatures (20, 80, 120, and 200 K) in the region of the  ${}^6H_{5/2} \rightarrow {}^6F_{5/2}$  transitions of  $\text{Sm}^{3+}$  and (b) the level diagram explaining the used designations of the spectral lines in the paramagnetic phase and the exchange splitting at a magnetic ordering.

of the erbium-probe line, this shift accompanied by a sharp narrowing of the line below the temperature  $T_3$  (Fig. 14) may indicate a change in the splitting of the ground-state Kramers doublet of the  $\text{Er}^{3+}$  ion with subsequent depopulation of the upper component of the doublet. We note that such a picture is typical for spin-reorientation phase transitions due to the anisotropy of the  $g$  factor in low-symmetry RE optical centers.

### 3. Spectra of $\text{Cr}^{3+}$ in $\text{SmCr}_3(\text{BO}_3)_4$

The optical spectrum of the transition-metal chromium ion  $\text{Cr}^{3+}$  with the  $3d^3$  outer electronic shell consists of weak narrow lines originating from spin-forbidden transitions

and broad bands corresponding to spin-allowed transitions. Figure 15 shows the spectrum of  $\text{Cr}^{3+}$  in  $\text{SmCr}_3(\text{BO}_3)_4$  up to  $19\,500\text{ cm}^{-1}$ . Energies of the chromium levels determined from the spectra are listed in Table III.

## V. MODELING OF SPECTRA AND MAGNETIC CHARACTERISTICS OF $\text{SmCr}_3(\text{BO}_3)_4$

### A. CF levels of the samarium and chromium ions

The electronic structure and magnetic properties of the  $\text{Sm}^{3+}$  and  $\text{Cr}^{3+}$  ions in the CFs of the  $D_3$  and  $C_2$  symmetry, respectively, in  $\text{SmCr}_3(\text{BO}_3)_4$  crystals with the  $R32$  structure,

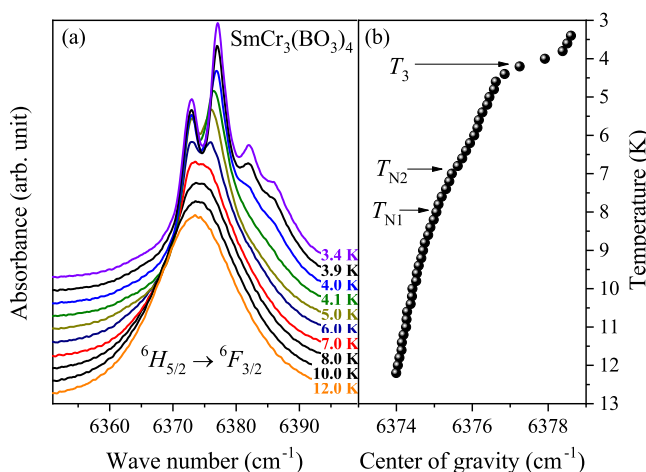


FIG. 13. (a) Line IB corresponding to the  $\Gamma_4({}^6H_{5/2}) \rightarrow \Gamma_{56}({}^6H_{15/2})$  transition in the low-temperature absorption spectra of a  $\text{SmCr}_3(\text{BO}_3)_4$  single crystal at different temperatures and (b) the temperature dependence of the position of the center of gravity for this line.

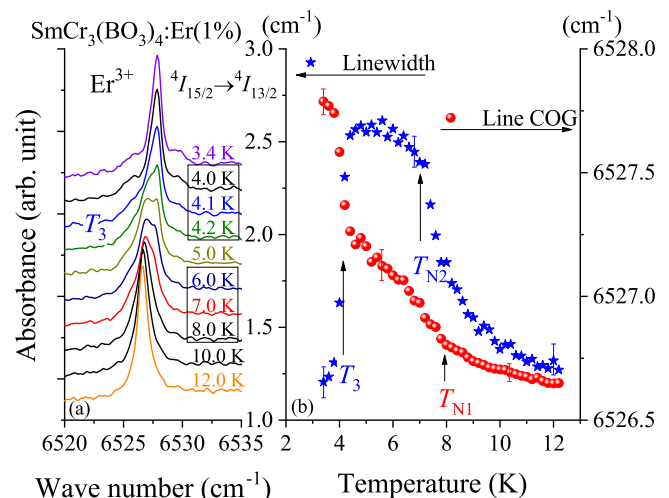


FIG. 14. (a) Spectral line IA of the  ${}^4I_{15/2} \rightarrow {}^4I_{13/2}$  transition in the  $\text{Er}^{3+}$  ion introduced as a probe into a  $\text{SmCr}_3(\text{BO}_3)_4$  single crystal at different temperatures and (b) the temperature dependence of the position of the center of gravity and halfwidth for this line.

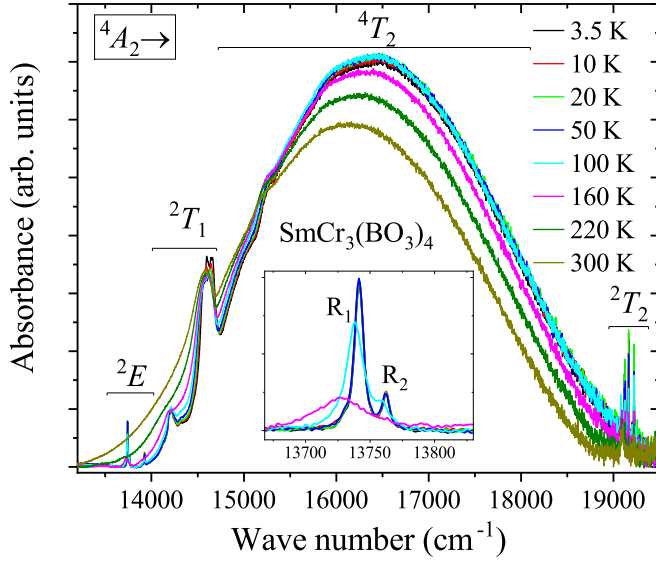


FIG. 15. Absorption spectra of a  $\text{SmCr}_3(\text{BO}_3)_4$  crystal at different temperatures in the region of optical transitions of the  $\text{Cr}^{3+}$  ions. The final states for optical transitions from the ground  $^4A_2$  state of  $\text{Cr}^{3+}$  are indicated.

are considered in this paper using the single-ion Hamiltonians  $H_{\text{Sm}}$  and  $H_{\text{Cr}}$ . The operators  $H_{\text{Sm}}$  and  $H_{\text{Cr}}$  are defined in full basis sets of 2002 and 120 states, corresponding to the ground  $4f^5(\text{Sm}^{3+})$  and  $3d^3(\text{Cr}^{3+})$  electronic configurations, respectively.

TABLE III. Energy levels ( $\text{cm}^{-1}$ ) of the  $\text{Cr}^{3+}$  ion in a CF of the  $C_2$  symmetry.

	$\text{YAl}_3(\text{BO}_3)_4:\text{Cr}^{3+}$		$\text{SmCr}_3(\text{BO}_3)_4$		
			(this paper)		
	Experiment		Theory		
	[37]	[8]	this paper	Experiment	Theory
$^4F\ ^4A_2$	0		0	—	0
	1.05		0.758	—	0.8697
$^2G\ ^2E\ R_1$	14 641	14 652	14 635	13 742	13 896
$^2G\ ^2E\ R_2$	14 695		14 670	13 761	13 923
$^2G\ ^2T_1$	15 275		15 224	14 221	14 476
	15 321		15 376	14 601	14 600
	15 375		15 575	14 653	14 848
			15 791		15 277
$^4F\ ^4T_2$			15 804		15 285
	16 950	16 750	16 167		15 778
			16 187	16 427	15 796
			16 595		16 944
			16 613		16 953
$^2G\ ^2T_2$			20 932	19 121	19 978
	20 846		21 774	19 167	20 870
			22 080	19 222	21 155
			22 323		21 875
$^4F\ ^4T_1$			22 328		21 893
	23 750	23 640	23 436		22 964
			23 448		22 965
			23 490		23 495
			23 498		23 502

Three  $\text{Sm}^{3+}$  ions in a unit cell are magnetically equivalent. The Hamiltonian of samarium ions has the form

$$H_{\text{Sm}} = H_{\text{FI}} + H_{\text{CF}} + H_Z, \quad (1)$$

where  $H_{\text{FI}}$  is a free-ion Hamiltonian [38],

$$H_{\text{FI}} = \sum_{k=2,4,6} F^k f_k + \zeta \sum_j \mathbf{I}_j \mathbf{s}_j + \alpha \mathbf{L}^2 + \beta G(G_2) + \gamma G(G_7) \\ + \sum_{k=2,3,4,6,7,8} T^k t_k + \sum_{k=0,2,4} M^k m_k + \sum_{k=2,4,6} P^k p_k, \quad (2)$$

the operator  $H_{\text{CF}}$  determines the ion energy in the CF in a Cartesian coordinate system with the  $z$  and  $x$  axes along the  $c$  and  $a$  crystallographic axes, respectively:

$$H_{\text{CF}} = B_0^2 C_0^{(2)} + B_0^4 C_0^{(4)} + B_0^6 C_0^{(6)} + iB_{-3}^4 [C_{-3}^{(4)} + C_3^{(4)}] \\ + iB_{-3}^6 [C_{-3}^{(6)} + C_3^{(6)}] + B_6^6 [C_{-6}^{(6)} + C_6^{(6)}], \quad (3)$$

(here,  $B_k^p$  are CF parameters and  $C_k^{(p)}$  are spherical tensor operators); the Zeeman operator  $H_Z$  is responsible for the interaction of an ion with a local magnetic field  $\mathbf{B}_{\text{loc}}$ :

$$H_Z = \sum_j \mu_B (\mathbf{I}_j + 2\mathbf{s}_j) \mathbf{B}_{\text{loc}}. \quad (4)$$

The summation in Eq. (4) is over  $4f$  electrons with orbital and spin moments  $\mathbf{I}_j$  and  $\mathbf{s}_j$ , respectively, and  $\mu_B$  is the Bohr magneton. The parameters of the Hamiltonian  $H_{\text{FI}}$  obtained from the comparison of the calculated spectra of the  $\text{Sm}^{3+}$  ions with the measurement data are (in  $\text{cm}^{-1}$ )  $F^2 = 78951$ ,  $F^4 = 56783$ , and  $F^6 = 40002$  (parameters of two-electron electrostatic interactions);  $\zeta = 1167$  (constant of the spin-orbit interaction);  $\alpha = 20.16$ ,  $\beta = -567$ , and  $\gamma = 1500$  (parameters of two-electron correlations between electronic configurations);  $P^2 = 357$ ,  $P^4 = 268$ ,  $P^6 = 178$ ,  $M^0 = 2.6$ ,  $M^2 = 1.46$ , and  $M^4 = 0.81$  (parameters of relativistic spin-orbital and magnetic interactions); and  $T^2 = 304$ ,  $T^3 = 36$ ,  $T^4 = 56$ ,  $T^6 = -347$ ,  $T^7 = 373$ , and  $T^8 = 348$  (parameters of three-particle interactions). In Eq. (2),  $\mathbf{L}$  is the total orbital angular momentum of electrons;  $G(G_2)$  and  $G(G_7)$  are the Casimir operators; and the operators  $f_k$ ,  $t_k$ ,  $m_k$ , and  $p_k$  are defined in Ref. [38].

Nine  $\text{Cr}^{3+}$  ions in the unit cell are divided into three groups of three ions, which form helical chains propagating along the  $c$  axis, connected by successive rotations through an angle of  $2\pi/3$  around the  $c$  axis passing through the samarium ions. Three sublattices of chromium ions, successively shifted along the  $c$  axis by  $\frac{1}{3}$  of the lattice constant  $c$  and forming a chain, are magnetically nonequivalent; the  $C_2$  symmetry axes at the positions of neighboring chromium ions in the chain are rotated in the  $ab$  plane by angles  $\pm 2\pi/3$ . For each of the three nonequivalent sublattices, we introduce a local Cartesian coordinate system with the  $Z$  axis along the local symmetry axis  $C_2$  and the  $X$  axis directed against the crystallographic  $c$  axis.

We represent the Hamilton operator of the  $3d^3$  electronic shell of the  $\text{Cr}^{3+}$  ion in the form

$$H_{\text{Cr}} = H_{ee} + H_{\text{SO}} + \alpha L(L+1) + H_{\text{CF}} + H_Z, \quad (5)$$

where  $H_{ee}$  is the energy of the electrostatic interactions between electrons,  $H_{\text{SO}}$  is the energy of the spin-orbit

TABLE IV. CF parameters (cm<sup>-1</sup>) in  $RM_3(\text{BO}_3)_4$  crystals.

$p q$	$B_q^p, \text{Sm}^{3+}$		$p q$	$B_q^p, \text{Cr}^{3+}$	
	$\text{SmFe}_3(\text{BO}_3)_4$ [35]	$\text{SmCr}_3(\text{BO}_3)_4$ this paper		$\text{YAl}_3(\text{BO}_3)_4$ this paper	$\text{SmCr}_3(\text{BO}_3)_4$ this paper
2 0	502	464	2 0	-2768	-2009.4
4 0	-1048	-1096	2 2	1302	1817.7
4 -3	575	614.7	2 -2	704	1576.5
6 0	432	402	4 0	-10 272	-11 012
6 -3	87	92.4	4 2	7534	7498
6 6	290	309.5	4 -2	25 064	25 014
			4 4	-14 117	-13 852
			4 -4	6856	6196.2

interaction, and  $\alpha$  is the Tris parameter. The operator of interaction with the CF in local coordinate systems has the form

$$\begin{aligned}
H_{\text{CF}} = & B_0^2 C_0^{(2)} + B_2^2 [C_{-2}^{(2)} + C_2^{(2)}] + iB_{-2}^2 [-C_{-2}^{(2)} + C_2^{(2)}] \\
& + B_0^4 C_0^{(4)} + B_2^4 [C_{-2}^{(4)} + C_2^{(4)}] + iB_{-2}^4 [-C_{-2}^{(4)} + C_2^{(4)}] \\
& + B_4^4 [C_{-4}^{(4)} + C_4^{(4)}] + iB_{-4}^4 [-C_{-4}^{(4)} + C_4^{(4)}]. \quad (6)
\end{aligned}$$

In calculations, we used the values of Slater parameters  $F^2 = 78\,157\text{ cm}^{-1}$ ,  $F^4 = 50\,331\text{ cm}^{-1}$ ,  $\alpha = 54\text{ cm}^{-1}$ , and the spin-orbit interaction constant  $\zeta = 195\text{ cm}^{-1}$ , obtained from the analysis of the absorption spectra of  $\text{SmCr}_3(\text{BO}_3)_4$ .

When simulating the measured optical spectra, the initial values of the CF parameters at the positions of the  $\text{Sm}^{3+}$  and  $\text{Cr}^{3+}$  ions were calculated within the framework of the exchange-charge model [39] using the structural parameters of the  $\text{SmCr}_3(\text{BO}_3)_4$  crystal lattice from Ref. [31]. These CF parameters were then corrected based on the measured data. The results of the variation are presented in Table IV, where for comparison, the CF parameters for  $\text{Sm}^{3+}$  in the isostructural crystal  $\text{SmFe}_3(\text{BO}_3)_4$  and for impurity  $\text{Cr}^{3+}$  ions in yttrium aluminum borate are also given.

The calculated energies of the CF levels of the lower multiplets of  $\text{Sm}^{3+}$  ions in the paramagnetic phase of  $\text{SmFe}_3(\text{BO}_3)_4$  are compared in Table II with the results of optical spectroscopy measurements on  $\text{Sm}M_3(\text{BO}_3)_4$  ( $M = \text{Cr}, \text{Fe}$ ) crystals. Table II also shows the calculated values of  $g$  factors ( $g_{\parallel} = g_{cc}$ ,  $g_{\perp} = g_{aa} = g_{b^*b^*}$ ) for Kramers doublets of  $\text{Sm}^{3+}$  ions in  $\text{SmCr}_3(\text{BO}_3)_4$  at temperatures  $T > T_{N1}$ . It is worth noting a strong mixing of the wave functions of the states belonging to the  ${}^6F_{1/2}$ ,  ${}^6F_{3/2}$ , and  ${}^6H_{15/2}$  multiplets in a CF.

The CF energies of the  ${}^4F$  and  ${}^2G$  terms of the  $\text{Cr}^{3+} 3d^3$  shell, calculated using the CF parameters given in Table IV for  $\text{Cr}^{3+}$  ions in  $\text{SmCr}_3(\text{BO}_3)_4$  and  $\text{YAl}_3(\text{BO}_3)_4:\text{Cr}^{3+}$  crystals, are compared in Table III with the measured energies of the maxima of broad electronic-vibrational bands and the energies of zero-phonon spin-forbidden transitions in the absorption spectra of chromium ions in  $\text{SmCr}_3(\text{BO}_3)_4$ . The dominant role in the formation of the spectrum of chromium ions is played by the cubic CF component, which splits the lower term  ${}^4F$  into the orbital singlet  ${}^4A_2$  (ground state) and triplets  ${}^4T_2$  and  ${}^4T_1$ .

The magnetic properties of the  $\text{Cr}^{3+}$  ion are determined by the parameters of the effective spin Hamiltonian  $H_S$  (spin  $S = \frac{3}{2}$ ) of the ground spin quadruplet, split by the trigonal CF component and spin-orbit interaction into two doublets. In the local coordinate system introduced above, with the axes  $X, Y$ , and  $Z \parallel C_2$ , in a magnetic field  $\mathbf{B}$ , the spin Hamiltonian has the form

$$\begin{aligned}
H_S = & D \left[ S_Z^2 - \frac{S(S+1)}{3} \right] \\
& + \mu_B (g_X B_X S_X + g_Y B_Y S_Y + g_Z B_Z S_Z). \quad (7)
\end{aligned}$$

Here,  $2|D|$  is a splitting of the quadruplet in zero magnetic field; we find  $D = -0.435\text{ cm}^{-1}$  using the experimental data presented in Table III. The matrices of the components of the effective magnetic moment  $\mathbf{M}_{\text{Cr}}$  of the chromium ion were calculated using the eigenfunctions of the operator  $H_{\text{Cr}}$  (at  $H_Z = 0$ ), corresponding to the four lower eigenvalues of this operator. The eigenvalues  $g_{\alpha} m$  ( $m = \pm \frac{3}{2}, \pm \frac{1}{2}$ ) of the operators  $M_{\text{Cr},\alpha}$  determine the values of the  $g$  factors in the spin Hamiltonian,  $g_X = 1.9703$ ,  $g_Y = 1.9673$ , and  $g_Z = 1.9637$ , which agree well with the measured  $g$  factors of impurity  $\text{Cr}^{3+}$  ions in  $\text{YAl}_3(\text{BO}_3)_4$  crystal ( $g_{\alpha\alpha} = 1.978 \pm 0.005$  [37] and  $g_{\alpha\alpha} = 1.971 \pm 0.005$  [40]) and in the magnetically concentrated crystal  $\text{YCr}_3(\text{BO}_3)_4$  ( $g_{\alpha\alpha} = 1.976$  [25]).

### B. Magnetic properties of helical chromium chains

The magnetic characteristics of the chromium subsystem in  $\text{SmCr}_3(\text{BO}_3)_4$  were considered within the framework of the self-consistent four-particle cluster model developed earlier in the theoretical study of the magnetic properties of isostructural yttrium [41] and erbium [42] iron borates. Considering isotropic exchange interactions  $H_{12} = -2J_{12}\mathbf{S}_{\text{Cr}1}\mathbf{S}_{\text{Cr}2}$  between neighboring magnetic ions in the chromium chain [ $J_{12}(R_{mn}) = J_{mn}$ ] and between the nearest  $\text{Cr}^{3+}$  ions in neighboring chains [ $J_{12}(R_{mnn}) = J_{mnn}$ ], the Hamiltonian of a cluster containing four neighboring chromium ions, acting in the space of  $4^4 = 256$  states of spin quadruplets, in the paramagnetic phase in an external uniform magnetic field  $\mathbf{B}$  can be represented in the form

$$\begin{aligned}
H_{\text{Cl,eff}} = & H_{\text{Cl}}^{(0)} + H_{\text{ex}} + H'_{\text{ex}} - (\mathbf{M}_1 + \mathbf{M}_4)(\mathbf{B} + \Delta\mathbf{B}) \\
& - (\mathbf{M}_2 + \mathbf{M}_3)\mathbf{B}. \quad (8)
\end{aligned}$$



Here, the operator  $H_{\text{Cl}}^{(0)}$  determines energy levels of the four noninteracting  $\text{Cr}^{3+}$  ions in a cluster corresponding to the initial splitting of the quadruplets  $2|D|$ ,  $\mathbf{M}_k$  are the operators of the magnetic moments of two outer ( $k = 1, 4$ ) and two internal ( $k = 2, 3$ )  $\text{Cr}^{3+}$  ions in local coordinate systems defined above (see Sec. V A). The magnetic field  $\Delta B$  additionally introduced in Eq. (8) acting on the outer ions is determined from the condition that the average values of the magnetic moments of all ions in the cluster should be equal. In Eq. (8),  $H_{\text{ex}}$  is the Hamiltonian of the exchange interactions within a cluster:

$$H_{\text{ex}} = -2J_{nn}(\mathbf{S}_1\mathbf{S}_2 + \mathbf{S}_2\mathbf{S}_3 + \mathbf{S}_3\mathbf{S}_4). \quad (9)$$

The operator  $H'_{\text{ex}}$  contains the energy of exchange interactions of two outer  $\text{Cr}^{3+}$  ions with their nearest neighbors in a chain as well as the energy of exchange interactions of all four cluster ions with their neighboring ions in the nearest chains in the self-consistent molecular-field approximation:

$$H'_{\text{ex}} = -2J_{nn}(\mathbf{S}_1 + \mathbf{S}_4)\langle\mathbf{S}\rangle - 4J_{nn} \sum_{j=1,2,3,4} \mathbf{S}_k\langle\mathbf{S}\rangle. \quad (10)$$

A relatively small difference between the Néel temperatures of  $\text{SmCr}_3(\text{BO}_3)_4$  ( $T_{\text{N1}} = 7.8$  K) and  $\text{LaCr}_3(\text{BO}_3)_4$  ( $T_{\text{N}} = 8.5$  K [28]) with the  $R32$  structure evidences a weak influence of a RE subsystem on magnetic properties of chromium chains. Assuming that the magnetic moments of  $\text{Cr}^{3+}$  ions antiferromagnetically order along the crystallographic  $a$  axis with decreasing temperature similarly to moments of iron ions in RE iron borates, the phase transition temperature  $T_{\text{N1}}$  can be found as the point of divergence in the antiferromagnetic susceptibility  $\chi_{\text{af}}(T)$  (a response of the system on the corresponding staggered magnetic field  $B_a$  at the positions of  $\text{Cr}^{3+}$  ions when the cluster Hamiltonian is represented by Eq. (8) with the reversed signs of operators  $M_{2a}$ ,  $M_{4a}$ , and  $S_{2a}$ ,  $S_{4a}$ ). Schemes for calculating the paramagnetic and antiferromagnetic susceptibilities within the self-consistent four-particle cluster model are given in Ref. [41]. The values of the two variable parameters  $J_{nn} = -2.55$  K and  $J_{nnn} = -0.98$  K were obtained from the condition  $\chi_{\text{af}}(T_{\text{N1}})^{-1} = 0$  and by comparing the calculated temperature dependences of the components of the static magnetic susceptibility tensor  $\chi_{\parallel}(T)$  and  $\chi_{\perp}(T)$  with the measurement data at  $T > T_{\text{N1}}$  (see Fig. 4). It should be noted that both obtained exchange integrals have the same signs and correspond to intrachain and interchain antiferromagnetic interactions, in contrast to the previously proposed interchain ferromagnetic interaction in chromium borates of samarium [30], gadolinium [26], terbium [27], and lanthanum [28]. However, in the framework of the four-particle cluster approach, which is a minimal cluster model not allowing a long-range magnetic ordering in a spin chain in absence of the interchain interactions, contrary to dimer or single-site mean field approximations used in previous studies [26–28,30], we must introduce the antiferromagnetic interchain interactions to obtain the observed magnetic phase transition.

Further, using the above values of the exchange integrals and the cluster Hamiltonian of Eq. (8) in the absence of an external field, we performed a self-consistent calculation of the average values of the spin projections of  $\text{Cr}^{3+}$  ions on the

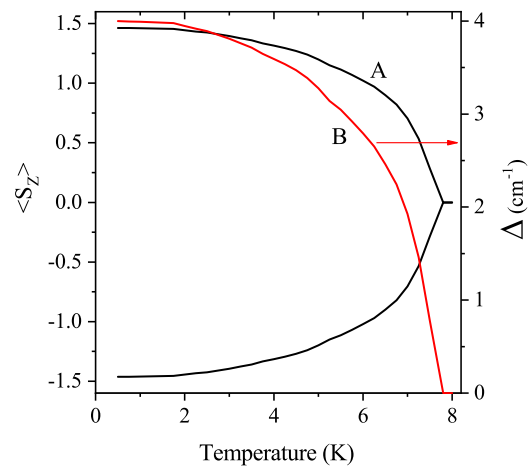


FIG. 16. Calculated temperature dependences of the (A) spin moment  $\langle S_Z \rangle$  of the  $\text{Cr}^{3+}$  ions and (B) ground-state splitting for the  $\text{Sm}^{3+}$  ions in an exchange field created by ordered chromium magnetic moments in  $\text{SmCr}_3(\text{BO}_3)_4$ .

$a$  axis,  $\langle S_Z \rangle(T)$ , as a function of temperature  $T < T_{\text{N1}}$  under the condition of equal absolute values and opposite signs of the spin moments of neighboring ions in the considered chain and of the nearest ions in neighboring chains. The calculation results are shown in Fig. 16.

### C. Modeling of the magnetic dc susceptibility and magnetization

Magnetic properties of  $\text{SmCr}_3(\text{BO}_3)_4$  are determined by the interacting subsystems of  $\text{Cr}^{3+}$  and  $\text{Sm}^{3+}$  ions. Each  $\text{Sm}^{3+}$  ion is at the center of a trigonal prism formed by six  $\text{Cr}^{3+}$  ions at the distance of 0.374 nm belonging to three helical chains. At the Néel temperature  $T_{\text{N1}}$ , the chemical unit cell containing three  $\text{Sm}^{3+}$  ions and nine  $\text{Cr}^{3+}$  ions in the  $R32$  structure doubles along the  $c$  axis. The spontaneous magnetic moments of the  $\text{Cr}^{3+}$   $nn$  ions (shifted relative each other by  $c/3$  along the  $c$  axis within helical chains) and of the  $nnn$  ions in neighbor chains are aligned antiparallel along the  $a$  axis. We suppose that, like the magnetic structure of the iron subsystem in iron borates [41], the chromium magnetic moments order ferromagnetically in the  $ab$  planes. In this case, the magnetic moments of  $\text{Cr}^{3+}$  ions at the vertices of regular triangles forming the rotated relative to each other's bases of  $\text{SmCr}_6$  prisms and containing the  $nnnn$  ions in the  $ab$  planes displaced relative to each other by  $2c/3$  along the  $c$  axis have the same directions.

Because of small Landé factors  $g_{\text{Sm}}$  and large distances ( $>0.6$  nm) between the  $\text{Sm}^{3+}$  ions, we can neglect interion interactions in the samarium subsystem. However, in the antiferromagnetic phase, magnetic moments on  $\text{Sm}^{3+}$  ions are induced by the ordered chromium subsystem. We introduce the isotropic exchange interaction between the nearest-neighbor  $\text{Sm}^{3+}$  and  $\text{Cr}^{3+}$  ions  $H_{fd} = -2J_{fd}\mathbf{S}_{\text{Cr}}\mathbf{S}_{\text{Sm}}$ , where the exchange integral  $J_{fd}$  is considered as the fitting parameter. In the mean-field approximation, the effective Hamiltonian of  $\text{Sm}^{3+}$  ions takes the form

$$H_{\text{Sm,eff}} = H_{\text{Sm}} - 12J_{fd} \langle \mathbf{S}_{\text{Cr}} \rangle \cdot \mathbf{S}_{\text{Sm}}, \quad (11)$$

where the operator  $H_{\text{Sm}}$  is given above in Eq. (1). The exchange field splits all Kramers doublets in the energy spectrum of  $\text{Sm}^{3+}$  ions at temperatures below  $T_{\text{N1}}$ . The absolute value of the exchange integral  $J_{fd} = 0.15$  K used in the further modeling of magnetic properties was obtained from a comparison of the calculated splitting  $\Delta$  of the  $\text{Sm}^{3+}$  ground state with the measured one at low temperatures [see Fig. 13(a)]. The procedure for calculating  $\Delta$  consisted of a numerical diagonalization of the Hamiltonian in Eq. (11) with the substituted values of the spontaneous spin moments  $\langle S_Z \rangle$  of  $\text{Cr}^{3+}$  ions along the  $a$  axis presented in Fig. 16(A) for varied values of  $J_{fd}$ . The calculated temperature dependence of this splitting is shown in Fig. 16(B). Next, the positive sign of  $J_{fd}$  corresponding to a ferromagnetic coupling between the  $\text{Sm}^{3+}$  and  $\text{Cr}^{3+}$  ions was found from the analysis of the measured dc susceptibilities of  $\text{SmCr}_3(\text{BO}_3)_4$ .

For the trigonal  $R32$  structure, components of the bulk susceptibility tensor  $\chi_{\parallel} = \chi_{cc}$  and  $\chi_{\perp} = (\chi_{aa} + \chi_{b^*b^*})/2$ . This equality follows from the trigonal symmetry in the paramagnetic phase, but it is also valid in the magnetically ordered phase under the assumption of the formation of domains with the orientation of magnetic moments along the three symmetry axes  $C_2$ . We simulated  $\chi_{\parallel}$ ,  $\chi_{\perp}$ , and the components of the magnetization vector  $M_a = M_{b^*}$  and  $M_c$  considering the coupled self-consistent equations for the magnetic moments of the  $\text{Sm}^{3+}$  and  $\text{Cr}^{3+}$  ions induced by the external magnetic fields directed along the crystallographic axes [42]. The quantum-statistical averaging of the  $\text{Sm}^{3+}$  magnetic moment was performed using the Hamiltonian of Eq. (11), and for the  $\text{Cr}^{3+}$  ions, we used the cluster Hamiltonian of Eq. (8) with additional terms corresponding to the exchange interactions between the  $\text{Cr}^{3+}$  and  $\text{Sm}^{3+}$  ions. The simulation results are shown in Figs. 4 and 6 together with measurement data. The simulated temperature dependences of both the longitudinal and transverse susceptibilities, as well as the field dependences of the magnetization, are in good agreement with the experimental data. The existing small discrepancies between the measured and calculated dependences are possibly related to the fact that the model considers only isotropic exchange interactions. It should be noted that, despite a strong suppression of the  $\text{Cr}^{3+}$  magnetic moments by interchain antiferromagnetic exchange interactions, the contributions of the chromium subsystem to the bulk magnetization are dominant (up to 96% of the measured values).

To analyze and interpret the observed specific features of the field dependences of magnetization at low temperatures, shown in Figs. 5 and 7, additional measurements of neutron diffraction in the samples under study are required to obtain information on the actual content of the trigonal and monoclinic phases and on the corresponding magnetic structures.

## VI. CONCLUSIONS

We have performed a comprehensive study of  $\text{SmCr}_3(\text{BO}_3)_4$ —a compound from the family of functional RE borates with the type of structure of the natural mineral huntite. Like RE iron borates, RE chromium borates contain chains of magnetic  $d$  ions in the structure. The spectroscopic method has shown the possibility of the presence in one

single crystal of two polytypic phases—trigonal  $R32$  and monoclinic  $C2/c$ . The crystals used in this paper were grown under conditions favorable for the preferential formation of the  $R32$  crystallographic phase; however, a presence of the  $C2/c$  phase could not be ruled out.

The heat capacity measurements revealed three phase transitions in a  $\text{SmCr}_3(\text{BO}_3)_4$  crystal, at the temperatures  $T_{\text{N1}} = 7.8 \pm 0.5$  K,  $T_{\text{N2}} = 6.7 \pm 0.5$  K, and  $T_3 = 4.3 \pm 0.2$  K. The first two are of the second-order type, while the lowest-temperature one has the features of a first-order phase transition.

The magnetic susceptibilities along the  $c$  and  $b^*$  directions [ $\chi_{\parallel}(T)$  and  $\chi_{\perp}(T)$ , respectively] coincide at  $T \geq 35$  K and follow the Curie-Weiss law with the negative Weiss temperature  $\Theta \approx -18$  K, which points to the predominantly antiferromagnetic exchange interactions. A quasi-one-dimensionality of the chromium magnetic subsystem manifests itself by broad maxima in the  $\chi(T)$  and  $C_p(T)$  dependences. Based on the magnetic measurement data, it was concluded that the temperature  $T_{\text{N1}}$  corresponds to an antiferromagnetic ordering of the easy-plane type,  $T_{\text{N2}}$  most likely relates to the Néel temperature of the impurity monoclinic phase  $C2/c$ , but the phase transition at  $T_3$  cannot be a spin reorientation of chromium ions to the  $c$  axis. A formation of some helical or noncollinear structure below  $T_3$  seems possible, but the exact nature of this transition is not clear. Measurements of the magnetoelectric effect on a mosaic of equally oriented crystals demonstrated an appearance of the magnetic-field-induced electric polarization at  $T_3$ . We also cannot exclude a symmetry-allowed piezoelectric contribution to the observed complex anomaly in the charge behavior at the transition at  $T_3$ .

Polarized temperature-dependent transmission spectra of a paramagnetic  $\text{SmCr}_3(\text{BO}_3)_4$  single crystal are well interpreted in the frame of a single  $\text{Sm}^{3+}$  center with the  $D_3$  point symmetry group, which shows that the trigonal  $R32$  phase dominates in the crystal. We found the energies and symmetries of 41 CF level of  $\text{Sm}^{3+}$  and, on that basis, performed CF calculations, determined CF parameters, and calculated magnetic  $g$  factors of samarium CF levels. The exchange splitting  $4 \text{ cm}^{-1}$  of the ground  $\Gamma_4$  Kramers doublet at the lowest temperature was found from the analysis of the spectral line splitting. In the spectral characteristics of  $\text{SmCr}_3(\text{BO}_3)_4$  crystals, pure and doped with a probe ion  $\text{Er}^{3+}$ , the most pronounced changes are observed at the temperature  $T_3$ . We also measured the spectra of  $\text{Cr}^{3+}$  in  $\text{SmCr}_3(\text{BO}_3)_4$ , determined the CF energies up to  $19\,500 \text{ cm}^{-1}$ , performed CF calculations, and found CF parameters for  $\text{Cr}^{3+}$  in  $C_2$ -symmetry positions of  $\text{SmCr}_3(\text{BO}_3)_4$ .

Further, the magnetic characteristics of the chromium subsystem in  $\text{SmCr}_3(\text{BO}_3)_4$  were considered within the framework of the self-consistent four-particle cluster model developed earlier, which is a minimal cluster model not allowing a long-range magnetic ordering in a spin chain in absence of the interchain interactions. The exchange integrals  $J_{nn} = -2.55$  K,  $J_{nm} = -0.98$  K, and  $J_{fd} = 0.15$  K between neighboring ions in the chromium chain, between the nearest  $\text{Cr}^{3+}$  ions in neighboring chains, and between the nearest-neighbor  $\text{Sm}^{3+}$  and  $\text{Cr}^{3+}$  ions, respectively, were obtained by comparing the calculated and measured data. Using the above values of the isotropic exchange integrals, the temperature

dependences of longitudinal and transversal susceptibilities, as well as the field dependences of magnetization, were successfully simulated. It was found that, despite a strong suppression of the  $\text{Cr}^{3+}$  magnetic moments by the inter-chain antiferromagnetic exchange interactions, the chromium subsystem gives a dominant contribution into the bulk magnetization of  $\text{SmCr}_3(\text{BO}_3)_4$ .

Further neutron and x-ray scattering measurements as well as calorimetry in a magnetic field, dielectric, and magneto-electric investigations are necessary to accurately determine the magnetic structures below the Néel temperature and  $B$ - $T$

phase diagrams for the  $R32$  and  $C2/c$  structural phases of  $\text{SmCr}_3(\text{BO}_3)_4$ .

#### ACKNOWLEDGMENTS

This paper was supported by the Russian Science Foundation under Grants No. 19-12-00413 (spectroscopy and theoretical modeling), No. 16-12-10531 (magnetic and magneto-electric measurements), and No. 19-12-00235 (study of phase formation and crystal growth). S.Y.G. acknowledges the use of the LPI Shared Facility Centre equipment.

- 
- [1] N. I. Leonyuk and L. I. Leonyuk, Growth and characterization of  $\text{RM}_3(\text{BO}_3)_4$  crystals, *Progr. Cryst. Growth Charact.* **31**, 179 (1995).
- [2] E. L. Belokoneva, M. A. Simonov, A. V. Pashkova, T. I. Timchenko, and N. V. Belov, Crystal structure of high-temperature monoclinical modification of  $\text{NdAl}_3(\text{BO}_3)_4$ , *Dokl. Akad. Nauk SSSR* **255**, 854 (1980) [*Sov. Phys. Dokl.* **25**, 948 (1980)].
- [3] E. L. Belokoneva, A. V. Pashkova, T. I. Timchenko, and N. V. Belov, Crystal structure of new monoclinic modification of high-temperature TRAl-borate  $\text{GdAl}_3(\text{BO}_3)_4$ , *Dokl. Akad. Nauk SSSR* **261**, 361 (1981) [*Sov. Phys. Dokl.* **26**, 1019 (1981)].
- [4] A. Brenier, C. Tu, Z. Zhu, and B. Wu, Red-green-blue generation from a lone dual-wavelength  $\text{GdAl}_3(\text{BO}_3)_4:\text{Nd}^{3+}$  laser, *Appl. Phys. Lett.* **84**, 2034 (2004).
- [5] P. Dekker, Ph. A. Burns, J. M. Dawes, J. A. Piper, J. Li, X. Hu, and J. Wang, Widely tunable yellow-green lasers based on the self-frequency-doubling material  $\text{Yb}:\text{YAB}$ , *J. Opt. Soc. Am. B* **20**, 706 (2003).
- [6] E. Bovero, Z. D. Luo, Y. D. Huang, A. Benayas, and D. Jaque, Single longitudinal mode laser oscillation from a neodymium aluminium borate stoichiometric crystal, *Appl. Phys. Lett.* **87**, 211108 (2005).
- [7] W. Ryba-Romanowski, R. Lisiecki, E. Beregi, and I. R. Martin, Spontaneous and stimulated emission in  $\text{Sm}^{3+}$ -doped  $\text{YAl}_3(\text{BO}_3)_4$  single crystal, *J. Lumin.* **167**, 163 (2015).
- [8] B. Malysa, A. Meijerink, and T. Justel, Temperature dependent luminescence  $\text{Cr}^{3+}$ -doped  $\text{GdAl}_3(\text{BO}_3)_4$  and  $\text{YAl}_3(\text{BO}_3)_4$ , *J. Lumin.* **171**, 246 (2016).
- [9] G. L. Reddy, L. R. Moorthy, P. Packiyaraj, and B. C. Jamalaih, Optical characterization of  $\text{YAl}_3(\text{BO}_3)_4:\text{Dy}^{3+}-\text{Tm}^{3+}$  phosphors under near UV excitation, *Opt. Mater.* **35**, 2138 (2013).
- [10] G. E. Malashkevich, V. N. Sigaev, N. V. Golubev, E. Kh. Mamadzhanova, A. V. Danil'chik, and E. V. Lutsenko, Rearrangement of optical centers and stimulated radiation of  $\text{Eu}^{3+}$  in polycrystalline huntite under optical and electron-beam excitation, *Pis'ma Zh. Eksp. Teor. Fiz.* **92**, 547 (2010) [*JETP Lett.* **92**, 497 (2010)].
- [11] N. N. Kuz'min, K. N. Boldyrev, N. I. Leonyuk, S. Yu. Stefanovich, and M. N. Popova, Luminescence and nonlinear optical properties of borates  $\text{LnGa}_3(\text{BO}_3)_4$  ( $\text{Ln} = \text{Nd}, \text{Sm}, \text{Tb}, \text{Er}, \text{Dy}, \text{or Ho}$ ), *Opt. Spektrosk.* **127**, 112 (2019) [*Opt. Spectrosc.* **127**, 107 (2019)].
- [12] K.-C. Liang, R. P. Chaudhury, B. Lorenz, Y. Y. Sun, L. N. Bezmaternykh, V. L. Temerov, and C. W. Chu, Giant magnetoelectric effect in  $\text{HoAl}_3(\text{BO}_3)_4$ , *Phys. Rev. B* **83**, 180417(R) (2011).
- [13] A. M. Kadomtseva, Yu. F. Popov, G. P. Vorob'ev, N. V. Kostyuchenko, A. I. Popov, A. A. Mukhin, V. Yu. Ivanov, L. N. Bezmaternykh, I. A. Gudim, V. L. Temerov, A. P. Pyatakov, and A. K. Zvezdin, High-temperature magnetoelectricity of terbium aluminum borate: the role of excited states of the rare-earth ion, *Phys. Rev. B* **89**, 014418 (2014).
- [14] N. V. Volkov, I. A. Gudim, E. V. Eremin, A. I. Begunov, A. A. Demidov, and K. N. Boldyrev, Magnetization, magnetoelectric polarization, and specific heat of  $\text{HoGa}_3(\text{BO}_3)_4$ , *Pis'ma Zh. Eksp. Teor. Fiz.* **99**, 72 (2014) [*JETP Lett.* **99**, 67 (2014)].
- [15] A. M. Kadomtseva, Yu. F. Popov, G. P. Vorob'ev, A. P. Pyatakov, S. S. Krotov, K. I. Kamilov, V. Yu. Ivanov, A. A. Mukhin, A. K. Zvezdin, A. M. Kuz'menko, L. N. Bezmaternykh, I. A. Gudim, and V. L. Temerov, Magnetoelectric and magnetoelastic properties of rare-earth ferrobates, *Fiz. Nizk. Temp.* **36**, 640 (2010) [*Low Temp. Phys.* **36**, 511 (2010)].
- [16] R. P. Chaudhury, F. Yen, B. Lorenz, Y. Y. Sun, L. N. Bezmaternykh, V. L. Temerov, and C. W. Chu, Magnetoelectric effect and spontaneous polarization in  $\text{HoFe}_3(\text{BO}_3)_4$  and  $\text{Ho}_{0.5}\text{Nd}_{0.5}\text{Fe}_3(\text{BO}_3)_4$ , *Phys. Rev. B* **80**, 104424 (2009).
- [17] T. Kurumaji, K. Ohgushi, and Y. Tokura, Magnetoelectric responses from the respective magnetic  $R$  and Fe subsystems in the noncentrosymmetric antiferromagnets  $R\text{Fe}_3(\text{BO}_3)_4$  ( $R = \text{Eu}, \text{Gd}, \text{and Tb}$ ), *Phys. Rev. B* **89**, 195126 (2014).
- [18] Y. Hinatsu, Y. Doi, K. Ito, M. Wakeshima, and A. Alemi, Magnetic and calorimetric studies on rare-earth iron borates  $\text{LnFe}_3(\text{BO}_3)_4$  ( $\text{Ln} = \text{Y}, \text{La-Nd}, \text{Sm-Ho}$ ), *J. Solid State Chem.* **172**, 438 (2003).
- [19] A. N. Vasil'ev and E. A. Popova, Rare-earth ferrobates  $R\text{Fe}_3(\text{BO}_3)_4$ , *Fiz. Nizk. Temp.* **32**, 968 (2006) [*Low Temp. Phys.* **32**, 735 (2006)].
- [20] M. N. Popova, Optical spectroscopy of low-dimensional rare-earth iron borates, *J. Magn. Magn. Mater.* **321**, 716 (2009).
- [21] V. S. Kurazhkovskaya, E. A. Dobretsova, E. Yu. Borovikova, V. V. Mal'tsev, and N. I. Leonyuk, Infrared spectroscopy and the structure of rare-earth chromium borates  $R\text{Cr}_3(\text{BO}_3)_4$  ( $R = \text{La-Er}$ ), *Zh. Strukt. Khim.* **52**, 721 (2011) [*J. Struct. Chem.* **52**, 699 (2011)].
- [22] E. Yu. Borovikova, E. A. Dobretsova, K. N. Boldyrev, V. S. Kurazhkovskaya, V. V. Maltsev, and N. I. Leonyuk,

- Vibrational spectra and factor group analysis of rare-earth chromium borates,  $RCr_3(BO_3)_4$ , with  $R = \text{La-Ho}$ , *Vib. Spectrosc.* **68**, 82 (2013).
- [23] E. A. Popova, N. I. Leonyuk, M. N. Popova, E. P. Chukalina, K. N. Boldyrev, N. Tristan, R. Klingeler, and B. Buechner, Thermodynamic and optical properties of  $\text{NdCr}_3(\text{BO}_3)_4$ , *Phys. Rev. B* **76**, 054446 (2007).
- [24] K. N. Boldyrev, E. P. Chukalina, and N. I. Leonyuk, Spectroscopic investigation of rare-earth chromium borates  $RCr_3(\text{BO}_3)_4$  ( $R = \text{Nd, Sm}$ ), *Fiz. Tverd. Tela* **50**, 1617 (2008) [*Phys. Solid State* **50**, 1681 (2008)].
- [25] L. Gondek, A. Szytuła, J. Przewoźnik, J. Żukrowski, A. Prokhorov, L. Chernush, E. Zubov, V. Dyakonov, R. Duraj, and Yu. Tyvanchuk, On the peculiar properties of triangular-chain  $\text{EuCr}_3(\text{BO}_3)_4$  antiferromagnet, *J. Solid State Chem.* **210**, 30 (2014).
- [26] A. Bludov, Yu. Savina, M. Kobets, V. Khurstal'yov, V. Savitsky, S. Gnatchenko, T. Zajarniuk, A. Lynnyk, M. U. Gutowska, A. Szewczyk, N. Kuzmin, V. Mal'tsev, and N. Leonyuk, Features of magnetic and magnetoelectric properties, H-T phase diagram of  $\text{GdCr}_3(\text{BO}_3)_4$ , *J. Magn. Magn. Mater.* **512**, 167010 (2020).
- [27] N. N. Kuzmin, V. V. Maltsev, E. A. Volkova, N. I. Leonyuk, K. N. Boldyrev, and A. N. Bludov, Growth and spectroscopic and magnetic properties of  $\text{TbCr}_3(\text{BO}_3)_4$  crystals, *Neorg. Mater.* **56**, 873 (2020) [*Inorg. Mater.* **56**, 828 (2020)].
- [28] A. Bludov, Yu. Savina, V. A. Pashchenko, S. L. Gnatchenko, I. V. Kolodiy, V. V. Mal'tsev, N. N. Kuzmin, and N. I. Leonyuk, The magnetic properties of the  $\text{LaCr}_3(\text{BO}_3)_4$  crystal, *Fiz. Nizk. Temp.* **46**, 767 (2020) [*Low Temp. Phys.* **46**, 643 (2020)].
- [29] A. Bludov, Yu. Savina, V. A. Pashchenko, S. L. Gnatchenko, T. Zajarniuk, A. Lynnyk, M. U. Gutowska, A. Szewczyk, I. V. Kolodiy, V. V. Mal'tsev, N. N. Kuzmin, and N. I. Leonyuk, Magnetic properties of  $\text{DyCr}_3(\text{BO}_3)_4$  crystal, *Fiz. Nizk. Temp.* **46**, 829 (2020) [*Low Temp. Phys.* **46**, 697 (2020)].
- [30] E. A. Dobretsova, K. N. Boldyrev, M. N. Popova, S. Yu. Gavrilkin, A. A. Mukhin, V. Yu. Ivanov, V. V. Mal'tsev, N. I. Leonyuk, and B. Z. Malkin, Phase transitions and exchange interactions in the  $\text{SmCr}_3(\text{BO}_3)_4$  crystal, *EPJ Web Conf.* **132**, 02008 (2017).
- [31] E. A. Dobretsova, *Huntite-like rare-earth borates, Investigations by methods of vibrational spectroscopy (infrared and Raman) and the Rietveld method*, Diploma work, Lomonosov Moscow State University, 2013.
- [32] S. A. Klimin, A. B. Kuzmenko, M. A. Kashchenko, and M. N. Popova, Infrared study of lattice dynamics and spin-phonon and electron-phonon interactions in multiferroic  $\text{TbFe}_3(\text{BO}_3)_4$  and  $\text{GdFe}_3(\text{BO}_3)_4$ , *Phys. Rev. B* **93**, 054304 (2016).
- [33] K. N. Boldyrev, N. N. Kuzmin, and E. A. Dobretsova, Structural specific features of solid solutions  $\text{Nd}_x\text{Gd}_{1-x}\text{Cr}_3(\text{BO}_3)_4$ , *Opt. Spektrosk.* **129**, 41 (2021) [*Opt. Spectrosc.* **129**, 37 (2021)].
- [34] I. V. Golosovsky, A. K. Ovsyannikov, D. N. Aristov, A. A. Mukhin, M. Boehm, L.-P. Regnault, and L. N. Bezmaternykh, Spin-wave dynamics and exchange interactions in multiferroic  $\text{NdFe}_3(\text{BO}_3)_4$  explored by inelastic neutron scattering, *J. Magn. Magn. Mater.* **451**, 443 (2018).
- [35] M. N. Popova, E. P. Chukalina, B. Z. Malkin, D. A. Erofeev, L. N. Bezmaternykh, and I. A. Gudim, Investigation of crystal field and exchange interactions in the  $\text{SmFe}_3(\text{BO}_3)_4$  multiferroic, *Zh. Eksp. Teor. Fiz.* **145**, 128 (2014) [*JETP* **118**, 111 (2014)].
- [36] M. N. Popova, High-resolution spectroscopy of rare earth cuprates and nickelates, *J. Alloys and Compounds* **275**, 142 (1998).
- [37] J.-P. R. Wells, M. Yamaga, T. P. J. Han, and M. Honda, Electron paramagnetic resonance and optical properties of  $\text{Cr}^{3+}$  doped  $\text{YAl}_3(\text{BO}_3)_4$ , *J. Phys.: Condens. Matter* **15**, 539 (2003).
- [38] W. T. Carnall, G. L. Goodman, K. Rajnak, and R. S. Rana, A systematic analysis of the spectra of the lanthanides doped into single crystal  $\text{LaF}_3$ , *J. Chem. Phys.* **90**, 3443 (1989).
- [39] B. Z. Malkin, Crystal field and electron-phonon interaction in rare-earth ionic paramagnet, in *Spectroscopy of Solids Containing Rare-Earth Ions*, edited by A. A. Kaplyanskii and R. M. Macfarlane (Elsevier Science, Amsterdam, 1987), Chap. 2, pp. 13–49.
- [40] A. D. Prokhorov, E. E. Zubov, A. A. Prokhorov, L. F. Chernush, R. Minyakaev, V. P. Dyakonov, and H. Szymczak, EPR spectra of  $\text{Cr}^{3+}$  ion in the Van Vleck paramagnet  $\text{EuAl}_3(\text{BO}_3)_4$ , *Phys. Status Solidi B* **250**, 1331 (2013).
- [41] B. Z. Malkin, E. A. Popova, E. P. Chukalina, A. Jablunovskis, and M. N. Popova, Self-consistent four-particle cluster model of  $\text{Fe}^{3+}$  Heisenberg chains: Spectral and magnetic properties of  $\text{YFe}_3(\text{BO}_3)_4$  crystals, *Phys. Status Solidi RRL* **14**, 1900603 (2020).
- [42] M. N. Popova, E. P. Chukalina, D. S. Erofeev, A. Jablunovskis, I. A. Gudim, and B. Z. Malkin, High-resolution optical spectroscopy and modeling of spectral and magnetic properties of multiferroic  $\text{ErFe}_3(\text{BO}_3)_4$ , *Phys. Rev. B* **101**, 205108 (2020).